

Few-Shot Object Detection: A Survey

Mona Köhler, Markus Eisenbach and Horst-Michael Gross

Abstract—Humans are able to learn to recognize new objects even from a few examples. In contrast, training deep-learning-based object detectors requires huge amounts of annotated data. To avoid the need to acquire and annotate these huge amounts of data, few-shot object detection aims to learn from few object instances of new categories in the target domain. In this survey, we provide an overview of the state of the art in few-shot object detection. We categorize approaches according to their training scheme and architectural layout. For each type of approaches, we describe the general realization as well as concepts to improve the performance on novel categories. Whenever appropriate, we give short takeaways regarding these concepts in order to highlight the best ideas. Eventually, we introduce commonly used datasets and their evaluation protocols and analyze reported benchmark results. As a result, we emphasize common challenges in evaluation and identify the most promising current trends in this emerging field of few-shot object detection.

Index Terms—Object Detection, Few-Shot Learning, Survey, Meta Learning, Transfer Learning

I. INTRODUCTION

In the last decade, object detection has tremendously improved through deep learning and, in particular, convolutional neural networks [1], [2]. However, deep-learning-based approaches typically require vast amounts of training data. Therefore, it is difficult to apply object detection to real-world scenarios involving novel objects that are not present in common object detection datasets. Annotating large amounts of images with bounding boxes or even segmentation masks is costly and tiresome. In some cases – such as medical applications [3] or the detection of rare species [4] – it is even impossible to acquire plenty of images.

Moreover, in contrast to typical deep-learning-based approaches, humans are able to learn new concepts with little data even at early age [5], [6], [7]. When children are shown new objects, they are able to recognize these objects even if they have seen them only once to a few times.

Therefore, a promising research area in this direction is few-shot object detection. Few-shot object detection aims at detecting novel objects with only few annotated instances after pretraining in the first phase on abundant publicly available data, as shown in Fig. 1. Consequently, it alleviates the burden of annotating large amounts of data in the target domain.

In this survey, we aim to provide an overview of state-of-the-art few-shot object detection approaches for new researchers in this emerging research field. First, we define the problem of few-shot object detection. Afterwards, we categorize current approaches and highlight similarities as

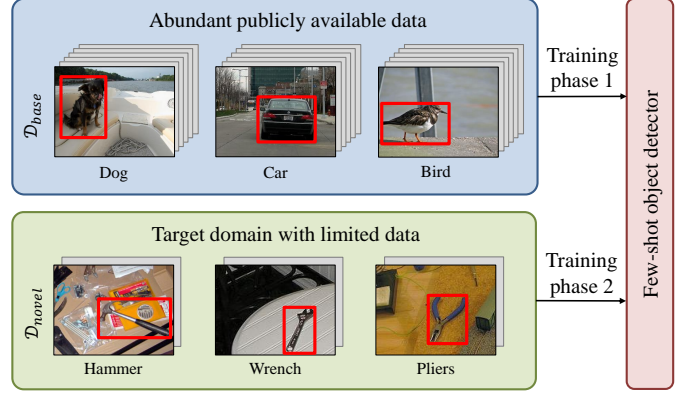


Fig. 1: General idea: By first training on a base dataset with abundant annotated bounding boxes, it is possible to apply few-shot object detectors to settings with only few annotated object instances, such as mechanical tools.

well as differences. We introduce commonly used datasets and their evaluation protocols. Subsequently, we compare the state-of-the-art approaches on these benchmarks. Finally, we emphasize common challenges in evaluation and identify promising research directions to guide future research.

II. PROBLEM DEFINITION

Few-shot object detection aims at detecting novel objects with only few annotated instances. Formally, the training dataset $\mathcal{D} = \mathcal{D}_{base} \cup \mathcal{D}_{novel}$ is separated into two datasets \mathcal{D}_{base} and \mathcal{D}_{novel} containing non-overlapping sets of base categories \mathcal{C}_{base} and novel categories \mathcal{C}_{novel} , with $\mathcal{C}_{base} \cap \mathcal{C}_{novel} = \emptyset$. Each tuple $(I_i, \hat{y}_{o_1}, \dots, \hat{y}_{o_M}) \in \mathcal{D}$ consists of an image $I_i = \{o_1, \dots, o_M\}$ containing M objects o_1, \dots, o_M and their corresponding labels $\hat{y}_{o_i} = \{c_{o_i}, b_{o_i}\}$, including the category c_{o_i} and the bounding box $b_{o_i} = \{x_{o_i}, y_{o_i}, w_{o_i}, h_{o_i}\}$ with coordinates (x_{o_i}, y_{o_i}) , width w_{o_i} , and height h_{o_i} . For the base categories \mathcal{C}_{base} abundant training data are available in the base dataset \mathcal{D}_{base} . In contrast, the novel dataset \mathcal{D}_{novel} contains only few annotated object instances for each novel category in \mathcal{C}_{novel} . For the task of K -shot object detection, there are exactly K annotated object instances available for each category in \mathcal{C}_{novel} . Therefore the number of annotated novel object instances $|\{o_j \in I_i \mid I_i \in \mathcal{D}_{novel}\}| = K \cdot |\mathcal{C}_{novel}|$ is relatively small. Note that the number of annotated object instances does not necessarily correspond to the number of images, as one image may contain multiple instances. N -way object detection denotes a detector that is designed to detect object instances from N novel categories, where $N \leq |\mathcal{C}_{novel}|$. Few-shot object detection is therefore often referred to as N -way K -shot detection.

Authors are with Neuroinformatics and Cognitive Robotics Lab, Ilmenau University of Technology, 98693 Ilmenau, Germany. mona.koehler@tu-ilmenau.de

This work has received funding from the Carl Zeiss Foundation as part of the project E4SM under grant agreement no. P2017-01-005.

Training an object detector only on \mathcal{D}_{novel} quickly leads to overfitting and poor generalization due to limited training data [8], [9]. However, training on the highly imbalanced combined data $\mathcal{D} = \mathcal{D}_{novel} \cup \mathcal{D}_{base}$ generally results in a detector that is heavily biased towards the base categories and, therefore, unable to correctly detect instances from novel categories [9]. Therefore, current research focuses on novel approaches for few-shot object detection. Typically, the initial detector model \mathcal{M}_{init} equipped with a backbone pretrained on classification data is first trained on \mathcal{D}_{base} , resulting in the base model \mathcal{M}_{base} . Most approaches then train \mathcal{M}_{base} on data $\mathcal{D}_{finetune} \subseteq \mathcal{D}$ including novel categories \mathcal{C}_{novel} , resulting in the final model \mathcal{M}_{final} :

$$\mathcal{M}_{init} \xrightarrow{\mathcal{D}_{base}} \mathcal{M}_{base} \xrightarrow{\mathcal{D}_{finetune}} \mathcal{M}_{final} \quad (1)$$

III. RELATED WORK ON TRAINING WITH LIMITED DATA

There are some related research areas that also focus on training with limited data. In the following, we will briefly discuss differences and similarities with few-shot object detection.

A. Few-Shot Learning and Classification

Before being applied to detection, few-shot learning was first explored for classification tasks [10], [11], [12], [13]. As objects with only few training instances do not need to be localized, classification is clearly easier. Yet, many ideas can be adopted for few-shot object detection.

B. Semi-Supervised Learning

Semi-supervised learning is related to few-shot learning in that only few labeled instances of the target categories are available. However, in contrast to few-shot learning, large amounts of additional unlabeled data are often available that help to learn appropriate representations [14], [15], [16].

Thus, when additional unlabeled data are available, methods from semi-supervised learning should be considered to improve the learned representations in few-shot learning approaches.

C. Generic Object Detection

Generic object detection is the joint task of localizing and classifying object instances of categories the detector was trained on. Regions of interest are localized by coordinates of bounding boxes and classified into a predefined set of categories. All other object categories which are not part of the training categories are regarded as background, and the detector is trained to suppress detections of those other categories. While achieving impressive results, these approaches require loads of annotated object instances per category and typically fail when applied to the few-shot regime.

Generic object detectors can be categorized into one-stage and two-stage detectors. Note that, one-stage detectors are also sometimes referred to as single-shot detectors. However, in this context, *shot* still refers to just one processing stage and not to the number of training examples.

One-stage detectors such as SSD [17], the YOLO series [18], [19], [20], [21] or RetinaNet [22] use a backbone network for feature extraction and do classification as well as bounding box regression directly on the extracted feature maps. In contrast, two-stage detectors such as R-CNN [23], Fast R-CNN [24] and the popular Faster R-CNN [25] first find regions of interest (RoIs) that can contain any object. Afterwards, these RoIs are classified and the bounding box parameters are adapted. A lot of approaches for few-shot object detection build upon Faster R-CNN [25], most often with a ResNet [26] as backbone. For higher detection rates, the backbone is often extended with a feature pyramid network (FPN) [27]. As this architecture is the basis for many few-shot object detection approaches, for researchers that are new in this field, we provide a more detailed description of Faster R-CNN in the appendix.

D. Zero-Shot Object Detection

Zero-shot object detection can be defined similar to few-shot object detection. However, as an extreme case, the number of annotated object instances is zero ($K=0$). Zero-shot detectors often incorporate semantic word embeddings [28], [29], i.e., semantically similar categories lead to similar features in the embedding space. This works for detecting everyday objects which can be easily labeled, but might be problematic when providing a specific label is difficult or when very similar objects need to be distinguished.

E. Object Detection for Long-tail Distributions

If a dataset has a long-tailed distribution of categories – such as LVIS [30] –, the detection of rare categories becomes difficult since the trained models are often biased towards the dominant categories. To perform well on all categories, approaches must address the problem of class imbalance [31], which is similar to the imbalance of base categories and novel categories in few-shot object detection. Therefore, concepts from long-tail distribution and few-shot learning might complement each other [32]. However, for datasets with long-tailed distributions, all categories are known from the beginning, whereas for few-shot learning / detection, novel categories with few instances are unknown during initial training (see Fig. 1).

F. Weakly Supervised Object Detection

Weakly supervised object detection relaxes the required annotations such that the training data contain only image-level labels, i.e., whether a specific object category is present or absent somewhere in the image [33], [34]. These annotations are much easier to obtain and can often be acquired by keyword search. The challenge for weakly supervised object detectors is detecting all object instances without having any localization information during training. Although alleviating the annotation burden, weakly supervised object detectors still require large amounts of images, which might be hard to obtain for detecting rare objects.

G. Class-agnostic Object Detection

Class-agnostic object detection is the task of localizing objects irrespective of their semantic category [35]. Implicitly, this requires the detector to find objects of categories, which were never seen during training. A class-agnostic object detector could be used as a preprocessing step for few-shot object detection. In the following step, the cropped objects merely would need to be classified, as in few-shot learning for classification.

In addition to the related research areas described above, in the following we will address learning techniques that are widely adopted in few-shot object detection.

H. Transfer Learning

Transfer learning refers to the re-use of network weights pretrained on a baseline dataset to improve generalization capabilities on a new domain with limited data. As in few-shot learning and detection, this usually involves novel categories from the target domain. However, unlike few-shot learning, the number of object instances for novel categories is not necessarily small. Therefore, techniques for learning from few data need to be incorporated in transfer learning approaches for few-shot object detection.

I. Metric Learning

Metric learning aims for learning an embedding in which inputs with similar content are encoded in features that have a small distance to each other in terms of the metric while encoded features from dissimilar inputs are supposed to be far apart [36]. To learn features with low inner-class and high inter-class ℓ^2 distances, triplet loss [37] or its extensions (see overview in [38]) are often used. Since this learned feature embedding typically generalizes well, the model can also be applied to encode instances of novel categories, which were unknown during training, and make metric-based decisions without the need for re-training. In the context of few-shot classification, this means that during inference the model extracts feature embeddings of the few annotated examples of \mathcal{D}_{novel} as well as of corresponding test images. The test image is then assigned to the category of the closest feature embedding of an annotated example. However, for few-shot detection, concepts for localizing instances in the images need to be integrated.

J. Meta Learning

Meta learning approaches learn how to learn in order to generalize for new tasks or new data [13]. For few-shot learning that means that these approaches learn how to learn to categorize the given inputs even though the categories are not fixed during training. These approaches need to learn how the required knowledge about the category is learned most efficiently, so that this category knowledge can also be learned for novel categories with few training examples.

IV. CATEGORIZATION OF FEW-SHOT OBJECT DETECTION APPROACHES

Approaches for few-shot object detection incorporate novel ideas in order to be able to detect objects with only few training examples. In general, the abundant training examples for base categories \mathcal{C}_{base} are used to leverage knowledge for the novel categories \mathcal{C}_{novel} with limited labeled data.

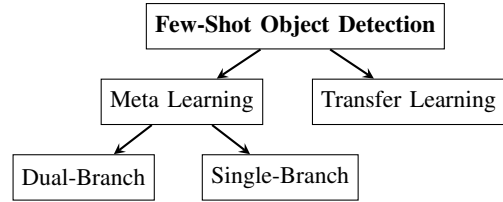


Fig. 2: Categorization of few-shot object detection approaches

We categorize approaches for few-shot object detection into meta learning and transfer learning approaches as shown in Fig. 2. We further divide meta learning approaches into single-branch and dual-branch architectures. Dual-branch architectures are constituted by a query and a support network branch, i.e. the network processes two inputs (a query and a support image) separately. Single-branch approaches in general resemble the architecture of generic detectors but reduce the number of learnable parameters when training on novel categories or utilize metric learning. Yet, also dual-branch architectures often incorporate ideas from metric learning.

In the appendix (Fig. 13), we show a diagram, that lists all approaches, that we cover in this survey sorted by year of publication and conference or journal, respectively. We can see that few-shot object detection is a rather young but emerging research field as most approaches have been published only within the last two years. Most approaches use transfer learning or dual-branch meta learning.

In the following, we first describe dual-branch meta learning approaches in section V. We start with the general training scheme for meta learning and follow with the typical realization. In the following subsections, we describe how specific approaches deviate from the general realization. In section VI we focus on single-branch meta learning approaches. Although there is no common realization from which others deviate, we still group approaches to their main ideas. In section VII we cover transfer learning approaches. Similarly to dual-branch meta learning approaches, we first describe the general realization and then turn to modifications.

Whenever appropriate, we give short take-aways at the end of the subsections in order to highlight key insights for well performing methods.

V. DUAL-BRANCH META LEARNING

A lot of approaches for few-shot object detection utilize meta learning in order to learn how to generalize for novel categories. In this section, we first describe the general training scheme for meta learning in subsection V-A. To realize meta learning, dual-branch approaches use a query and a support branch as we outline in subsection V-B. In the following subsections, we describe how specific approaches deviate from the general realization.

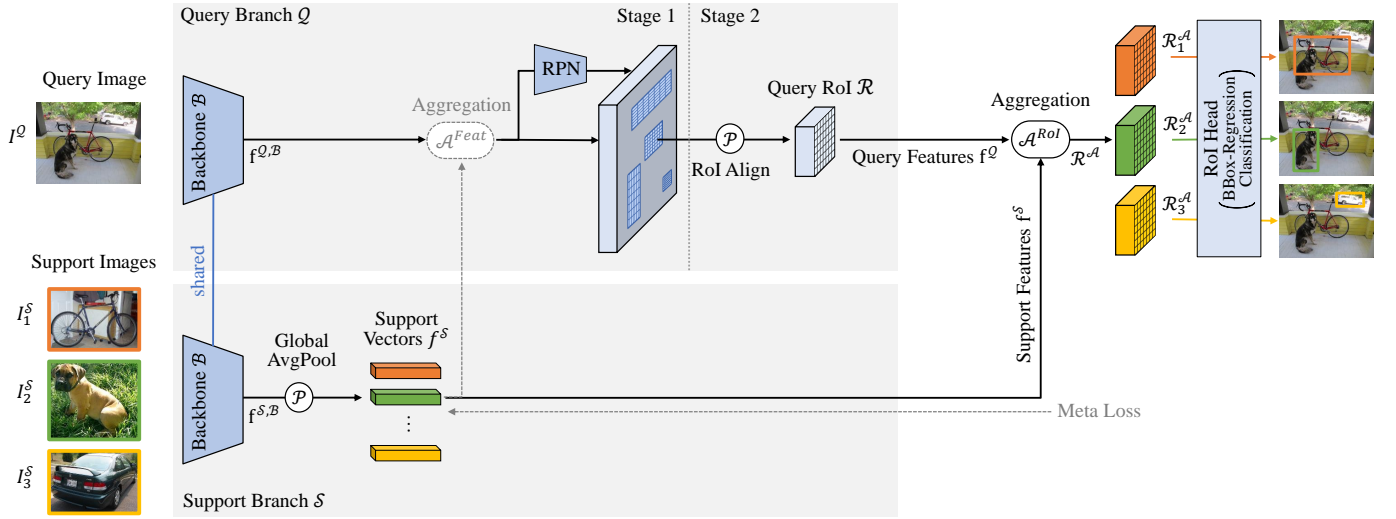


Fig. 3: General architecture with meta learning based on Faster R-CNN. Query and support images are fed through a shared backbone. The support features are pooled through global averaging and aggregated with the query features. We show here the 1-shot-3-way case without loss of generality.

A. Training Scheme

For meta learning, the model is trained in multiple stages. First of all, the model \mathcal{M}_{init} is trained only on the base dataset \mathcal{D}_{base} , resulting in \mathcal{M}_{base} . Typically, an episodic training scheme is applied, where each of the E episodes mimics the N -way- K -shot setting. This is called meta training. In each episode e (also known as few-shot task) the model is trained on K training examples of N categories on a random subset $\mathcal{D}_{meta}^e \subset \mathcal{D}_{base}$, $|\mathcal{D}_{meta}^e| = K \cdot N$. Therefore, the model needs to learn how to discriminate the presented categories in general depending on the input. Lastly, during meta finetuning the model \mathcal{M}_{base} is trained on the final task, resulting in \mathcal{M}_{final} .

$$\mathcal{M}_{init} \xrightarrow[e=1 \dots E]{\mathcal{D}_{meta}^e \subset \mathcal{D}_{base}} \dots \rightarrow \mathcal{M}_{base} \xrightarrow{\mathcal{D}_{finetune}} \mathcal{M}_{final} \quad (2)$$

If the model is supposed to detect both base and novel categories, it is trained on a balanced set $\mathcal{D}_{finetune} \subset \mathcal{D}$ of K training examples per category, irrespective if it is a base or a novel category. Otherwise, if we are only interested in the novel categories, the model is trained only on $\mathcal{D}_{finetune} = \mathcal{D}_{novel}$. Note that some approaches do explicitly not finetune on novel categories, but simply apply \mathcal{M}_{base} to novel categories, which is called meta testing. During meta testing, the model simply predicts novel objects in inference mode, when presented with K annotated examples of N categories.

B. General Realization

Dual-branch approaches utilize a two-stream architecture with one query branch \mathcal{Q} and one support branch \mathcal{S} as shown in Fig. 3. The input to the query branch \mathcal{Q} is an image I^Q on which the model should detect object instances, whereas the support branch \mathcal{S} receives the support set $\mathcal{D}^S = \{(I_i^S, \hat{y}_{o_j})\}_{i=1}^{K \cdot N}$, with K support images I_i^S for each of N categories and exactly one designated object o_j and its

label \hat{y}_{o_j} per image. There are, three options, how to present the designated object: First, all training examples are already cropped to the designated object by the ground truth bounding box, as shown in Fig. 3 bottom. Second, the full-size image and an additional binary mask, indicating the location of the object, is presented. Third, as in [39], the full-size image can be used and the region with features of the designated object is extracted by RoI Align [40]. For all three options, we refer to the presented image as support image I^S . A support image for a specific category c is denoted as $I^{S,c}$.

The support branch \mathcal{S} is now supposed to extract relevant features f^S of the support image I^S . These support features f^S are then aggregated with the features f^Q from the query branch \mathcal{Q} , denoted as $\mathcal{A}(f^Q, f^S)$, in order to guide the detector towards detecting object instances of category c from $I^{S,c}$ in the query image I^Q .

Note that the following explanation refers to the most basic and widely used architecture for few-shot object detection with meta learning that is depicted in Fig. 3. As shown in Fig. 4, the specific approaches may differ in one or multiple points described here and will be explained in detail in the following subsections.

Many approaches build on top of Faster R-CNN [25] with a ResNet [26] backbone. Often, a siamese backbone is utilized, i.e. the query branch \mathcal{Q} and the support branch \mathcal{S} share their weights. The backbone features $f^{Q,B}$ of the query branch \mathcal{Q} are further processed by a region proposal network (RPN) and a RoI align, resulting in the query RoIs \mathcal{R} . In the support branch \mathcal{S} , the support features from the backbone $f^{S,B}$ are pooled through global averaging, resulting in representative support vectors f^S for each category. In case of $K > 1$, for each category c the mean of its support vectors is calculated, resulting in one support vector $f^{S,c}$ per category. These support vectors encode category-specific information which are then used to guide the RoI head in recognizing objects of these categories. Therefore, query RoIs \mathcal{R} and support vectors f^S

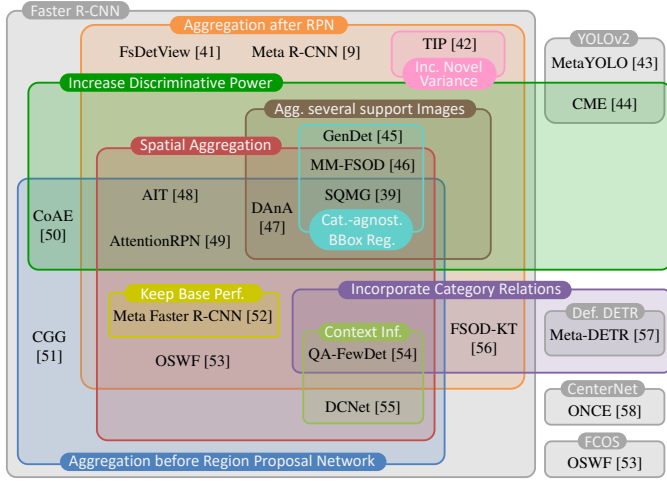


Fig. 4: Categorization of dual-branch meta learning approaches. Best viewed in color.

are aggregated – shown as \mathcal{A}^{RoI} in Fig. 3 –, in the most simple case by channel-wise multiplication \mathcal{A}_{mult} as in Eq. 3.

After aggregation, for each of the N categories there are separate RoIs $\mathcal{R}^{A,c}$. Their features are specialized for recognizing objects of the respective category c . These category-specific RoIs $\mathcal{R}^{A,c}$ are then fed into a shared RoI head for bounding box regression and binary classification. Since the aggregated RoIs $\mathcal{R}^{A,c}$ already contain category-specific information, the multi-category classification can be replaced by a binary classification that only outputs the information whether the RoI $\mathcal{R}^{A,c}$ contains an object of the specific category c or not. To enforce only one category for each RoI \mathcal{R} , a softmax layer can be applied afterwards.

Note that the RoI heads for all categories share the same weights. Therefore, the RoI head must generalize across categories. With this mechanism, it is theoretically possible to detect objects of novel categories without finetuning on novel categories, but simply meta testing. This makes meta-learning approaches especially useful for real-world applications, as no further training is required.

During inference, the support features f^S of the few images of \mathcal{D}_{novel} can be computed once for all N categories, such that the support branch \mathcal{S} is no longer required.

C. Variants for Aggregation

The particular dual-branch meta learning approaches differ most in the way the aggregation between query f^Q and support features f^S is implemented.

1) Aggregation before the Region Proposal Network:

Typically, the features of the query RoI \mathcal{R} are aggregated with the support vectors f^S . However, this requires the region proposal network (RPN) to output at least one RoI for each relevant object. Otherwise, even the best aggregation method can not help in recognizing the desired object. However, the RPN is trained only on base categories. If the novel categories \mathcal{C}_{novel} differ a lot from the base categories \mathcal{C}_{base} , the RPN

might fail to output suitable RoIs for recognizing objects of \mathcal{C}_{novel} . Therefore, as shown in Fig. 4, others aggregate the features before the region proposal network, which we denote by \mathcal{A}^{Feat} in Fig. 3.

Takeaway: When using Faster R-CNN as detector, an aggregation before the region proposal network leads to better region proposals, and thus less missed detections.

2) Aggregation Operation:

In the most simple case, the support vectors f^S and the query features f^Q are multiplied channel-wise:

$$\mathcal{A}_{mult}(f^Q, f^S) = f^Q \odot f^S \quad (3)$$

where \odot denotes the Hadamard product.

Moreover, different aggregation operations are explored in the state of the art. In GenDet [45] support features are convolved / correlated with the query features. Li *et al.* [53] (OSWF) use cosine similarity between each element of f^Q and f^S , which resembles \mathcal{A}_{mult} in Eq. 3, but with an additional scaling factor.

$$\mathcal{A}_{cos}(f^Q, f^S) = \frac{f^Q \odot f^S}{\|f^Q\| \cdot \|f^S\|} \quad (4)$$

Michaelis *et al.* [59] (OSIS), [51] (CGG) calculate the ℓ^1 -distance at each position and concatenate the resulting similarity features to the query features. Compared to cosine similarity, the ℓ^1 -distance is a different but also effective way to measure similarity. The query features themselves still contain relevant information. Afterwards, a 1×1 convolution (denoted by Φ_{comb}) is applied to halve the number of channels, such that it is equal to the initial number of channels.

$$\mathcal{A}_{\ell^1, Q}(f^Q, f^S) = \Phi_{comb} \left(\left[\left[f^Q - f^S \right], f^Q \right] \right) \quad (5)$$

where $[\cdot, \cdot]$ denotes channel-wise concatenation.

Xiao *et al.* [41] (FsDetView) use a more complex aggregation operation by combining channel-wise multiplication as in \mathcal{A}_{mult} with subtraction and query features themselves similar to $\mathcal{A}_{\ell^1, Q}$:

$$\mathcal{A}(f^Q, f^S) = \left[f^Q \odot f^S, f^Q - f^S, f^Q \right] \quad (6)$$

Meta Faster R-CNN [52] builds upon this aggregation,

$$\mathcal{A} = \left[\Phi_{Mult}(f^Q \odot f^S), \Phi_{Sub}(f^Q - f^S), \Phi_{Cat}[f^Q, f^S] \right] \quad (7)$$

where Φ_{Mult} and Φ_{Sub} and Φ_{Cat} each denote a small convolutional network with three conv and ReLU layers.

Fan *et al.* [49] (AttentionRPN) design an aggregation method which helps the detector to better discriminate different categories from each other. In AttentionRPN [49] the similarity of support features f^S and query RoIs \mathcal{R} are measured by global, local and patch-based attention modules. The outputs of all three matching modules are summed to give the final matching score.

Zhang *et al.* [39] (SQMG) decided to enhance the query features f^Q by support features f^S with dynamic convolution [60]. f^S is fed into a kernel generator to generate the weights of the

convolution. Afterwards, the generated weights are convolved with f^Q . Finally, the region proposal network is applied onto the enhanced features, resulting in region proposals which are more related to the presented category c of the support image $I^{S,c}$, and thus improves the recall. Moreover, after the RPN, the region proposals are compared with the support features utilizing a relation network [61]. Only those region proposals that exceed a prespecified score threshold and survive non maximum suppression are further considered.

Hsieh *et al.* [50] (CoAE) propose a co-attention method in order to make the query features f^Q attend to the support features f^S and vice versa. Therefore, two mutual non-local operations [62] Φ^Q and Φ^S are utilized which receive inputs from both f^Q and f^S . Afterwards, the outputs of the non-local operations are added to the inputs as a residual:

$$\begin{aligned} F^Q &= f^Q + \Phi^Q(f^Q, f^S) \\ F^S &= f^S + \Phi^S(f^S, f^Q) \end{aligned} \quad (8)$$

F^Q is fed into the RPN for computing region proposals which are able to better locate objects of the category c from the support image $I^{S,c}$. In order to further enhance the relatedness, Hsieh *et al.* [50] propose a subsequent squeeze-and-co-excitation method, which extends the squeeze-and-excitation of SENet [63]: With global average pooling and two fully-connected layers, a reweighting vector v is computed from F^S . The result is then used to re-weight the query features F^Q :

$$\tilde{F}^Q = v \odot F^Q \quad (9)$$

Finally, the computed region proposals are extracted from \tilde{F}^Q , resulting in RoIs $\mathcal{R}^{A,c}$ which are already tuned to the correct category c .

With AIT Chen *et al.* [48] push the idea of CoAE [50] a little further. Instead of using a single non-local block, multi-head co-attention is utilized for aggregating query and support features before the region proposal network. Let \mathbf{V} , \mathbf{K} and \mathbf{Q} be the value, key and query of a Transformer-based attention [64]. Similarly to the co-attention in CoAE, query features stem from another branch:

$$\begin{aligned} \mathbf{F}^Q &= \text{attention}(\mathbf{V}^Q, \mathbf{K}^Q, \mathbf{Q}^S) \\ \mathbf{F}^S &= \text{attention}(\mathbf{V}^S, \mathbf{K}^S, \mathbf{Q}^Q) \end{aligned} \quad (10)$$

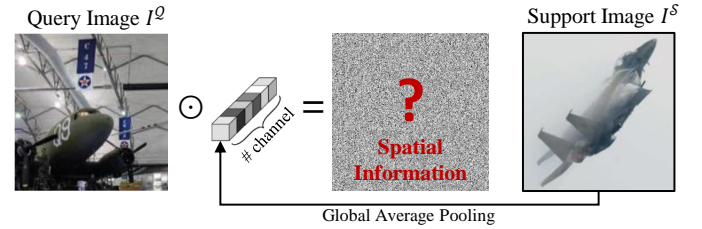
where superscripts Q and S denote whether features are from the query or support branch. The resulting features \mathbf{F}^Q encode related visual characteristics of both the query image I^Q and the support image I^S , which helps the region proposal network to predict RoIs related to I^S . According to Chen *et al.* [48], this improves the accuracy compared to the non-local attention block [62] in CoAE [50]. After the RPN, AIT [48] uses a transformer-based encoder-decoder architecture for transforming the RoIs \mathcal{R} to emphasize visual features corresponding to the given support image I^S .

Zhang *et al.* [57] (MetaDETR) first enhance query features with inter-class correlations as we will describe in subsection V-D. Afterwards, the features are aggregated similar to \mathbf{F}_s in Eq. 10.

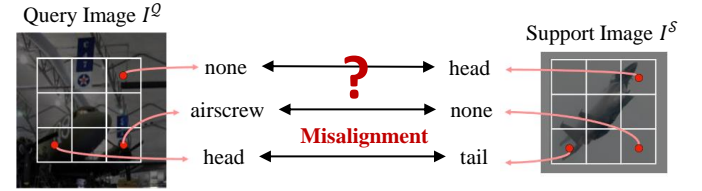
Takeaway: While earlier approaches design manually engineered aggregation methods, attention-based aggregations [62], [64] can better incorporate the relations of support and query features.

3) Keep Spatial Information for Aggregation:

As opposed to aggregating support features via average pooling, others (see Fig. 4) propose to utilize spatial information. For the object detection task, objects are located by bounding boxes. However, not every part of that bounding box is occupied by the object and, therefore, does not contain relevant information about the respective category. With average pooling however, these irrelevant features are aggregated into the support vector. Moreover, with global average pooling spatial information is completely lost, as illustrated in Fig. 5a.



(a) Loss of spatial information due to global average pooling.



(b) Spatial misalignment due to convolution-based aggregation.

Fig. 5: Common aggregation problems. Images based on DANa [47].

Therefore, Li *et al.* [53] (OSWF) first pool support features to the same spatial dimension as the query RoI \mathcal{R} . Afterwards, these pooled features are concatenated to the query RoI \mathcal{R} . Finally, 1×1 convolutions are used to compare structure-aware local features.

Chen *et al.* [47] argue that a convolution of query features f^Q and support features f^S is less suitable, since the objects in query images I^Q and support images I^S are generally not aligned in the same way, as shown in Fig. 5b. Therefore, by using dual-awareness attention (DANa) Chen *et al.* [47] first highlight relevant semantic features of the respective category on the support features f^S and suppress background information. Then, an attention-based aggregation is performed, incorporating the spatial correlations between f^Q and f^S .

Meta Faster R-CNN [52] first uses non-spatial aggregation for fusing query features f^Q and support features f^S before the region proposal network to create category-specific RoIs $\mathcal{R}^{A,c}$. Afterwards, an attention mechanism is used to first spatially align support and RoI features and second to focus on foreground regions. Finally, the resulting attentive RoI and support features are aggregated as depicted in Eq. 7.

Zhang *et al.* [39] (SQMG) implicitly incorporate spatial dimensions by utilizing a relation network [61] for aggregation.

Hu *et al.* [55] (DCNet) use an attention mechanism which extends the non-local self-attention mechanism [62]. In contrast to self-attention, the support features f^S modulate the query features f^Q , which can be regarded as cross-attention. A similar cross-attention is utilized by Hiseh *et al.* [50] (CoAE), as described in Eq. 8.

Chen *et al.* [48] (AIT) push the idea a little further, by incorporating multi-head co-attention as described in Eq. 10.

While using transformer-based attention mechanism [64], Zhang *et al.* [57] (MetaDETR) still first pool support features f^S to a vector before aggregating with query features f^Q . Yet, the authors argue that the multi-head attention modules before aggregation already encode both support f^S and query features f^Q into the same feature space.

Takeaway: The spatial information of a support image I^S , as well as its relation to a query image I^Q , is best incorporated through transformer-based attention mechanisms [62], [64].

4) Aggregation of Several Support Images:

In the general approach, to fuse all support images of category c , the mean of their features is calculated:

$$\{I_i^{S,c}\}_{i=1}^K : f^{S,c} = \frac{1}{K} \sum_{i=1}^K f_i^{S,c} \quad (11)$$

However, not all support images provide the same amount of information for the respective category as shown in Fig. 6. Unusual object views, object parts, or even occlusion by objects of other categories impair discriminative power if support features $f_i^{S,c}$ are simply averaged.

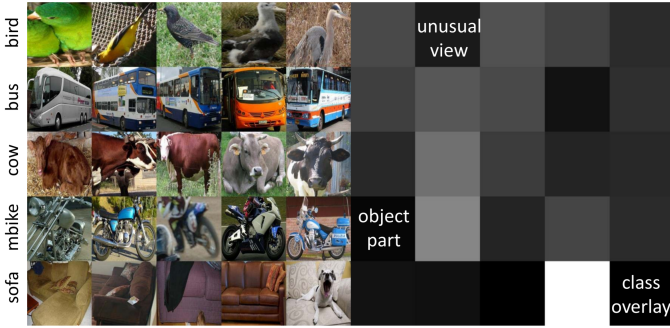


Fig. 6: Different amount of information for several support images of the same category. Image from GenDet [45].

Therefore, a weighted average is proposed in GenDet [45]. The weight w_i for each support image $I_i^{S,c}$ is computed by the similarity between the single-shot and the mean detector and learned during training.

$$\{I_i^{S,c}\}_{i=1}^K : f^{S,c} = \frac{1}{K} \sum_{i=1}^K w_i \cdot f_i^{S,c} \quad (12)$$

Both DAnA [47] and SQMG [39] incorporate the similarity of query f^Q and different support features f^S : In DAnA [47] support features $f_i^{S,c}$ of K different images $\{I_i^{S,c}\}_{i=1}^K$ are first aggregated independently with the query features f^Q based on the correlation between query and support. As the importance

of each support images $I_i^{S,c}$ is already incorporated, the resulting K aggregated features can be simply averaged:

$$\{I_i^{S,c}\}_{i=1}^K : \mathcal{A}(f^Q, f^{S,c}) = \frac{1}{K} \sum_{i=1}^K \mathcal{A}(f^Q, f_i^{S,c}) \quad (13)$$

In SQMG [39] the support features $f_i^{S,c}$ of multiple support images $I_i^{S,c}$ are weighted according to their similarity with the query features f^Q using an attention mechanism. First, the similarity is computed with a relation network [61]. Afterwards, the weighting values w_i for support features $f_i^{S,c}$ are computed with a softmax on the similarity score. The final support features are achieved by a weighted sum as in Eq. 12.

Takeaway: As not all support images provide the same amount of information, their individual relevance should be incorporated, as shown in Fig. 6.

D. Incorporate Relations between Categories

Han *et al.* [54] (QA-FewDet) highlight the problem that many dual-branch meta-learning approaches work as a kind of single-category detector without modeling multi-category relations. However, especially for novel categories resembling base categories, these relations can help in correctly classifying objects (e.g. a motorbike is more similar to a bicycle than to an airplane).

Therefore, in contrast to using visual features only, Kim *et al.* [56] (FSOD-KT) additionally incorporate linguistic features. Before aggregation, the support vectors f^S are fed through a knowledge transfer module which exploits semantic correlations between different categories. This knowledge transfer module is implemented by a graph convolutional network [65]. The input to this graph convolutional network is a graph where each node represents one category, and the values on the edges represent the similarities between linguistic category names. However, this is only applicable if all categories have predefined and distinct category names, and might be hard to transfer to, e.g., medical imaging.

Han *et al.* [54] (QA-FewDet) also utilize graph convolutions but do not rely on the linguistic category names. In contrast, they build a heterogeneous graph which enhances support vectors f^S with multi-category relations in order to better model their relations and incorporate features from similar categories. Moreover, their heterogeneous graph also aligns support and query features: Since the support features $f^{S,c}$ of one category c are only extracted from few support images, there might be a huge discrepancy to query RoIs \mathcal{R}^c that actually belong to the same category c . Therefore, the heterogeneous graph also contains pairwise edges between RoIs, in order to mutually adapt features of $f^{S,c}$ and \mathcal{R}^c and reduce their discrepancy.

Although not using graph convolutions, Zhang *et al.* [57] (MetaDETR) also incorporate relations between different categories by transforming their support features. The authors introduce a correlation aggregation module, which is able to simultaneously aggregate multiple support categories in order to capture their inter-class correlation. This helps in reducing misclassification and enhances generalization to novel categories. First, the query features f^Q are matched with multiple support features f^S simultaneously by utilizing attention

modules [64]. Afterwards, task encodings help to differentiate these support categories.

Takeaway: Incorporating the relations between different categories helps in better representing and classifying the data-sparse novel categories $\mathcal{C}_{\text{novel}}$.

E. Increase Discriminative Power

After aggregation, for each RoI \mathcal{R} , there exist N category-specific RoIs $\mathcal{R}^{A,c}$, which are classified independently. If the support features f^S for different categories are too similar, this independent classification might lead to ambiguities. Therefore, some approaches use an additional meta loss to enforce the support features f^S to be as diverse as possible. Most often (e.g. in [9], [41], [56], [42], [54]), the support features f^S are classified, and a simple cross-entropy loss is applied. This encourages the support vectors to fall in the category the respective object belongs to. More advanced approaches utilize techniques from metric learning to increase discriminative power, as described in the following.

GenDet [45] and MetaDETR [57] use a loss based on cosine similarity for more discriminative support vectors. First of all, the support vectors f^S are normalized. Afterwards, for each pair of support vectors (f^{S,c_i}, f^{S,c_j}) the cosine similarity is computed which results in a similarity matrix $A \in \mathbb{R}^{N \times N}$, where N is the number of different categories. With an ℓ^1 loss, the similarity matrix A is constrained to be close to the identity matrix $I_N \in \mathbb{R}^{N \times N}$. Intuitively speaking, this results in minimizing the similarity between different support vectors and maximizing the discriminative ability of each support vector, i.e., a high margin between different support vectors.

MM-FSOD [46] uses the pearson distance for aggregating f^S and f^Q . Compared to cosine similarity, Pearson distance first normalizes each dimension with the mean of all dimensions, resulting in a smaller inner-class variance. Therefore, there is no need for designing a special distance loss function, and the simple cross-entropy loss can be utilized.

Li *et al.* [44] (CME) propose an adversarial training procedure for min-max-margin: Next to a loss for increasing the margin, the features of novel categories are disturbed to reduce the discriminative power of their support vectors and, thus, decrease the margin. To be precise, the most discriminative pixels are erased in an adversarial manner by backpropagating the gradient to the input support image. With this approach, CME [44] is capable to accurately detect more objects with fewer false positives.

For the meta learning approach, the detector is supposed to detect objects in a query image I^Q that are of the same category c as the object in the support image $I^{S,c}$. Due to this problem definition, meta learning approaches tend to focus on separating foreground from background instead of distinguishing different categories, as noted by Zhang *et al.* [39] (SQMG). This often leads to false positives, i.e. predicted bounding boxes, even though the query image I^Q does not contain any instance of the regarded category c . However, it is equally important that the detector can distinguish different categories and identify which object categories are *not* present

in the query image. Therefore, in AttentionRPN [49] a two-way contrastive training strategy is proposed. In addition to a positive support image $I^{S,c}$, a negative support image $I^{S,n}$ is used from an object category $n \in \mathcal{C} \setminus \{c\}$ that is not present in the query image I^Q . This training strategy is adapted by DANa [47]. Zhang *et al.* [39] (SQMG) extend the contrastive loss with an adaptive margin [66] in order to separate the different categories by a proper distance. The adaptive margin incorporates semantic similarity of the categories by word embeddings [67].

A second problem highlighted by Zhang *et al.* [39] (SQMG) is the extreme imbalance of many background proposals vs. few foreground proposals, which impedes distance metric learning. To combat the foreground-background imbalance, the authors use a focal loss [22] which down-weights the easy background proposals and focuses on the hard negatives.

CoAE [50] uses an additional margin-based loss to improve the ranking of the regions of interest in the region proposal network. Those regions of interest with a high similarity to the object in the support image I^S should be at the top of the ranking, since only the top 128 RoIs will be further processed. Therefore, the authors designed a margin-based metric to predict the similarities for all regions of interest. Chen *et al.* [48] (AIT) adopt this margin-based ranking loss.

In typical episodic training, only N categories are presented in each episode. According to Liu *et al.* [45] (GenDet), this could lead to a low discriminative ability of the extracted features, as only the sampled categories are distinguished. Thus, their approach GenDet [45] utilizes an additional reference detector during training, where all base categories $\mathcal{C}_{\text{base}}$ need to be distinguished. The index of a specific base category stays the same over all episodes. Via an additional loss, both detectors are constrained to output similar results. This guides the backbone to extract more discriminative features.

Takeaway: In order to increase the discriminative power and differentiate between several categories, ideas from metric learning such as similarity metrics, as well as contrastive training should be employed.

F. Proposal-free Detectors

Most approaches build on top of the two-stage detector Faster R-CNN [25]. However, these approaches need to deal with possibly inaccurate region proposals and the decision of whether to aggregate support features f^S and query features f^Q before or after the region proposal network or both. When utilizing proposal-free detectors, f^S and f^Q can simply be aggregated after feature extraction and before classification and bounding box regression.

Some approaches utilize simple one-stage detectors, such as YOLOv2 [19] in MetaYOLO [43] and CME [44] or RetinaNet in DANa [47]. Others build on top of anchor-free detectors like CenterNet [68] in ONCE [58] or FCOS [69] in Li *et al.* [53] (OSWF) and GenDet [45]. The transformer-based detector Deformable DETR [70] is utilized in MetaDETR [57]. MetaDETR aggregates support features f^S and query features f^Q after the shared backbone. Subsequently, a category-agnostic transformer architecture predicts the objects.

Takeaway: While most approaches build on top of Faster R-CNN, proposal-free detectors are easier to implement. Especially transformer-based architectures will probably surpass other approaches in near future, as already observed in other vision domains [71].

G. Keep the Performance on Base Categories

In order to better detect base categories and prevent catastrophic forgetting, Han *et al.* [52] (Meta Faster R-CNN) use an additional branch following the original Faster R-CNN [25] architecture. As Meta Faster R-CNN already aggregates query features f^Q and support features f^S before the region proposal network, only the weights for the backbone are shared between those two branches. After meta training on the base categories \mathcal{C}_{base} , the weights of the backbone are fixed and the RPN and RoI head for the base category branch are trained. Finally, the other branch is adapted or simply applied to novel categories with meta finetuning or meta testing, respectively (see subsection V-A for terminology definitions). As the first branch stays fixed, the performance for base categories \mathcal{C}_{base} won't drop due to meta finetuning.

H. Increase the Variance of Novel Categories

TIP [42] expands the few training examples for novel categories with data augmentation techniques such as Gaussian noise or cutout. However, naively adding data augmentation impairs detection performance. Therefore, Li *et al.* [42] (TIP) use an additional transformed guidance consistency loss, implemented by ℓ^2 norm, which constrains support vectors f_i^S, f_j^S generated by original image I_i^S and transformed image $I_j^S = \phi(I_i^S)$ to be close to each other. This results in more similar and representative support vectors even for different support images, thus improving detection performance of novel categories. Moreover, during training, the query branch Q also receives transformed as well as original images. The features of the transformed query image I^Q are fed into the region proposal network to predict regions of interest (RoIs). These RoIs are then cropped from the features of the original non-transformed query image via RoI Align [40]. This forces the detector to predict consistent RoIs independent of the transformation used for the query image.

I. Incorporate Context Information

Typically, by applying RoI pool or RoI align, region proposals are pooled to a specific squared size of, e.g., 7×7 . However, this might lead to information loss during training, which could be remedied with abundant training data. With only few training examples available, this information loss could result in misleading detections. Therefore, DCNet [55] uses three different resolutions and performs parallel pooling. Similar to the pyramid pooling module in the PSPNet [72] for semantic segmentation, this helps to extract context information, where larger resolutions help to focus on local details, while smaller resolutions help to capture holistic information. In contrast to the pyramid pooling module, the branches are fused with attention-based summation.

Han *et al.* [54] (QA-FewDet) find that query RoIs \mathcal{R} might be noisy and may not contain complete objects. Therefore, they built a heterogeneous graph which uses graph convolutional layers [65]. Pairwise edges between proposal nodes incorporate both local and global context of different RoIs in order to improve classification and bounding box regression.

J. Category-agnostic Bounding Box Regression

Even though parameters for binary classification and bounding box regression are shared for all categories, most approaches compute them for each category-specific RoI independently. In contrast, GenDet [45], MM-FSOD [46] and SQMG [39] share the bounding box computation among different categories. This follows the intuition that even though different categories vary in their visual appearances, regression of bounding box values has common traits. Moreover, it saves computation overhead.

Conclusion on Dual-Branch Meta Learning Approaches

Dual-branch meta learning approaches are very common in few-shot object detection. They enable fast adaption for novel categories or can even be applied to novel categories without finetuning but with a simple forward pass, i.e., meta testing. This is especially useful for real-world applications.

However, they require a complex episodic training scheme, as described in subsection V-A. Moreover, with an increasing number of categories in the support set, more memory is required, since aggregation needs to be performed for each category individually.

VI. SINGLE-BRANCH META LEARNING

Single-branch architectures for few-shot object detection follow another approach. Since there are no query and support branches, the general architecture resembles the architecture for generic object detectors such as Faster R-CNN [25] (see Appendix). However, there is no single approach from which others deviate. Still, all approaches use episodic training as described in subsection V-A, which is typical for meta learning. In Fig. 7, we display our categorization of single-branch meta learning approaches, which we further describe in the following.

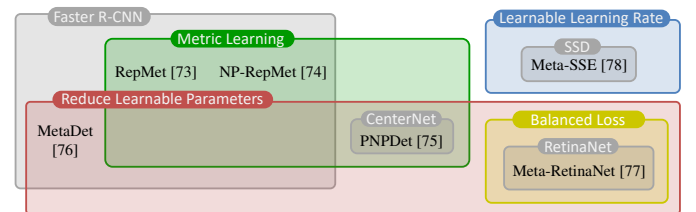


Fig. 7: Categorization of single-branch meta learning approaches. Best viewed in color.

A. Metric Learning

Similarly two dual-branch meta learning, metric learning plays a key role for single-branch approaches.

One of the first approaches for few-shot object detection – RepMet [73] – defines the few-shot object detection task as a distance metric learning problem. For localization, RepMet simply uses the regions of interest (RoIs) \mathcal{R} from Faster R-CNN [25]. With several fully-connected layers, RepMet computes embedded feature vectors f^+ of these RoIs \mathcal{R} . These feature vectors f^+ are then compared to representative vectors R_{ij}^+ , where i and j denote the i -th category and the j -th representative. These representative vectors R_{ij}^+ are learned via backpropagation. The highest similarity between the embedded feature vector f^+ and a representative vector R_{ij}^+ determines the category i for the RoI \mathcal{R} . If the similarity is too low, the RoI is rejected as background. To learn an adequate feature embedding, an additional embedding loss is used, which enforces a minimum margin between the distance of the embedded vector to the closest representative of the correct category and the distance to the closest representative of the wrong category. Thus, different categories can be distinguished better. During testing, the representatives R_{ij}^+ are replaced by embedded feature vectors f^+ of \mathcal{D}_{novel} .

RepMet uses the positive region proposals of a category, but discards its negative proposals. However, for learning the embedding space, negative – especially hard negative – proposals are essential. Therefore, in addition to learning positive embedded feature vectors f^+ and positive representative vectors R_{ij}^+ for each category i , NP-RepMet [74] also learns negative embedded feature vectors f^- and negative representative vectors R_{ij}^- per category. The embedding spaces for R_{ij}^+ and R_{ij}^- are learned by utilizing a triplet loss [37].

PNPDet [75] uses cosine similarity for distance metric learning of the objects' categories to allow for better generalization to novel categories. Moreover, cosine similarity can inherently model irrelevance for background regions. Cosine similarity computes the similarity of the input image's features with learned prototypes of each category. As the intra-class variances of different categories vary, an adaptive scaling factor for each category is learned as well.

Takeaway: Metric learning helps in creating more discriminative features for better distinguishing between different categories.

B. Reduce Learnable Parameters

Since few training examples of novel categories might not be sufficient to train a deep neural network, some approaches reduce the number of learnable parameters for few-shot fine-tuning.

Wang *et al.* [76] (MetaDet) introduce a weight-prediction meta model that learns how to generate category-specific weights in order to generalize for novel categories \mathcal{C}_{novel} with only few training examples. After training on the base dataset, category-agnostic weights (i.e. backbone and RPN of Faster R-CNN) are frozen, and an episodic training scheme is applied to learn how to predict category-specific weights for the base categories \mathcal{C}_{base} . Finally, during meta-testing, the meta model

predicts category-specific weights for the novel categories \mathcal{C}_{novel} . For inference, the meta model can be detached, and the detector looks like the standard Faster R-CNN.

Li *et al.* [77] (MetaRetinaNet) reduce the number of learnable parameters by freezing all backbone layers after training on \mathcal{D}_{base} and instead learn coefficient vectors v initialized to ones. These learnable coefficient vectors v are multiplied with the convolution weights w , resulting in a modified convolution operation: $f_{out} = f_{in} \otimes (w \odot v) \oplus b$.

Zhang *et al.* [75] (PNPDet) freeze the whole network after training on \mathcal{D}_{novel} . For few-shot finetuning, a second small sub-network is introduced for learning to classify the novel categories \mathcal{C}_{novel} . This disentangling of novel and base categories prevents a decreasing performance on base categories.

Takeaway: When training on data-scarce \mathcal{D}_{novel} , the number of learnable parameters should be reduced. However, simple transfer learning approaches (see section VII) that also reduce the number of learnable parameters are able to surpass the approaches presented here.

C. Learnable Learning Rate

Fu *et al.* [78] design their MetaSSD such that the model's parameters can adjust fast – with just one parameter update – to the novel categories \mathcal{C}_{novel} . All parameters from original SSD detector [17] get an additional learnable learning rate. During meta learning, these learning rates are learned individually by a meta learner from the distribution of the current task, resulting in neither overfitting nor underfitting.

D. Balanced Loss Function

Li *et al.* [77] (MetaRetinaNet) introduce a balanced loss, which reduces the performance imbalance of different tasks in meta learning. For meta training, in each episode different training examples of different categories are sampled, and they achieve different performances. This performance imbalance hinders stability and makes it difficult to adapt the model to novel categories. Thus, a balancing loss is introduced, which constrains the detector to achieve similar performance across episodes.

Conclusion on Single-Branch Meta Learning Approaches

Single-branch meta learning approaches are much less explored in few-shot object detection. Thus, more advanced dual-branch approaches or transfer learning approaches are able to surpass the approaches presented here.

VII. TRANSFER LEARNING

Meta learning approaches depend on a complex episodic training. In contrast, transfer learning approaches utilize a fairly simple two-phase approach on a single-branch architecture, most often a Faster R-CNN [25], as first proposed by Wang *et al.* [79] (TFA) and shown in Fig. 8.

In the first phase, the detector is trained on the base categories \mathcal{C}_{base} . Afterwards, all detector weights are frozen except for RoI head, which are responsible for bounding box regression and classification. In the second phase, transfer

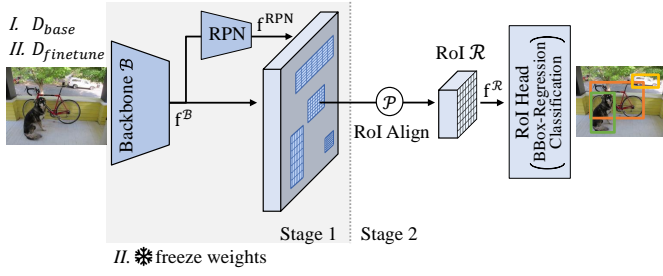


Fig. 8: Realization with transfer learning

learning is performed, by finetuning the last layers on the base categories \mathcal{C}_{base} and novel categories \mathcal{C}_{novel} . For finetuning, the training set is composed of balanced subsets of base category data \mathcal{D}_{base} and novel category data \mathcal{D}_{novel} with K shots for each of the base and novel categories. The only modification to Faster R-CNN is the use of cosine similarity for classification, which is crucial to compensate for differences in feature norms of base categories \mathcal{C}_{base} and novel categories \mathcal{C}_{novel} , as analyses in [80] have shown. Wang *et al.* [79] showed that this simple approach is sufficient to adequately learn the novel categories \mathcal{C}_{novel} and outperform earlier meta learning approaches that are more complex.

Building upon this simple approach, many modifications have been proposed. Fig. 9 shows all transfer learning approaches categorized by the architecture employed and by their modifications. Below, we describe all the proposed modifications, grouped by the categories shown.

A. Modifications of the Region Proposal Network

For the very few-shot setting, where the number of instances K for novel categories \mathcal{C}_{novel} is very low, the region proposal network (RPN) was identified as a key source for errors [81]. For example if the detector must learn to detect a category from a single example, the detector can model the categories' variation only by proposing multiple regions of interest (RoIs) that match the object's ground truth, which is similar to random cropping augmentation, as shown in [80] (see subsection VII-C). If the RPN misses even one of these RoIs, the performance on this novel category may drop noticeably. Therefore, Zhang *et al.* [81] (CoRPN) modify the RPN, by replacing the single binary foreground classifier in the RPN with M binary classifiers. The goal is that a least one classifier identifies the relevant RoI as foreground. By two loss terms, the M binary classifiers are trained to be distinct, but also to be cooperative in order to avoid missing too many boxes. As in TFA [79], in the second training phase, the weights of the RPN are frozen.

Fan *et al.* [82] (Retentive R-CNN) observed that the RPN suppresses RoIs of novel categories \mathcal{C}_{novel} after it was trained only on \mathcal{D}_{base} in the first phase. They found that unfreezing the weights of the RPN's final layer that classifies whether objects are foreground or background is sufficient to improve the RPN in the second phase. The same conclusion was drawn by Sun *et al.* [80] (FSCE) and as a result, all RPN weights were unfrozen. Additionally, they doubled the number of proposals that pass non-maximum suppression to get more proposals

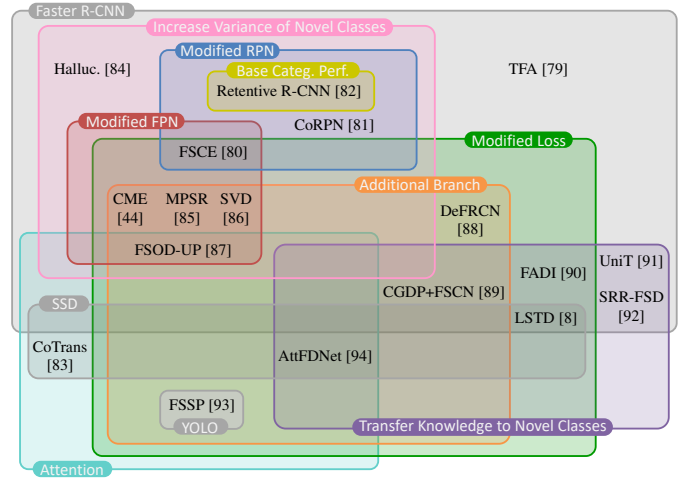


Fig. 9: Transfer learning approaches categorized by detector architecture and types of modifications. Best viewed in color.

for novel categories. They compensate for this by sampling only half the number of proposals in the RoI head used for loss computation, as they observed that in the second training phase the discarded half contains only backgrounds.

Takeaway: In order to reduce the number of missed detections, the region proposal network should be learned as well in the finetuning phase when training on \mathcal{D}_{novel} .

B. Modifications of the Feature Pyramid Network

Next to unfreezing the RPN, Sun *et al.* [80] (FSCE) showed that also finetuning the Feature Pyramid Network (FPN) in the second phase improves the performance compared to freezing its weights. They assume that the concepts from the base categories cannot be transferred to novel categories without any finetuning.

Wu *et al.* [85] (MPSR) observed that the distribution of object sizes of a specific category changes when only few instances are sampled, since the lack of instances leads to a sparse scale space. While the feature pyramid network (FPN) builds multi-scale feature maps to detect objects at different scales, it does not change the distribution in the data of novel categories and the sparsity of the scale distribution remains unsolved. Therefore, Wu *et al.* [85] propose multi-scale positive sample refinement (MPSR) that is applied in an auxiliary refinement branch and includes changes of the processing in the FPN. In the refinement branch, data augmentation shall compensate for the sparse scale space (see subsection VII-C).

Takeaway: FPN weights should be adapted during finetuning. Furthermore, to compensate for missing scales of novel categories, the processing pipeline of the FPN should be modified by a multi-scale positive sample refinement.

C. Increase the Variance of Novel Categories

If training instances for novel categories \mathcal{C}_{novel} are limited, also the variance of the data regarding these categories is limited. Therefore, some approaches try to increase the variance of the data for novel categories.

In the refinement branch of MPSR [85], each object is cropped by a square window and resized to various scales. This increases the variance regarding object sizes. For each scaling, two specific corresponding scale levels of the FPN are selected and their feature maps are forwarded to the RPN head and RoI head, respectively. These augmented scales compensate for the missing scales in the sparse distribution of novel categories. This positive sample refinement is also employed in FSOD-UP [87] and CME [44]. A similar approach is taken by Xu *et al.* [93] (FSSP), where in an auxiliary branch the objects are augmented regarding scale and translation, as shown in Fig. 10. Only one object is extracted and most background pixels are set to zero to force the network to focus on this foreground object.

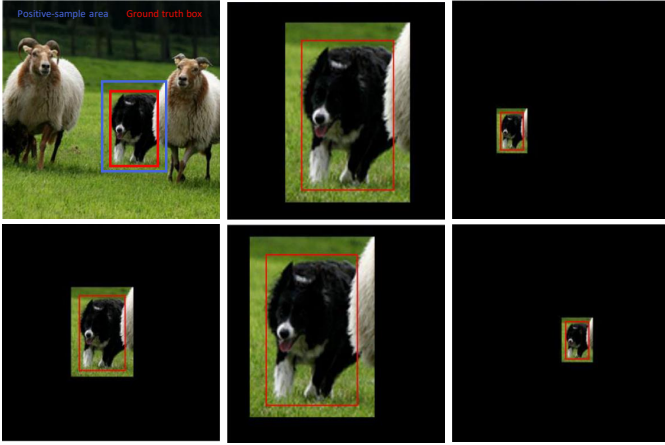


Fig. 10: Augmentation for novel categories regarding scale and translation in FSSP [93].

Zhang *et al.* [84] (Halluc.) introduce a hallucinator network that learns to generate additional examples for novel categories C_{novel} . Therefore, for features in the RoI head, a hallucinator network learns the shared within-class feature variation from base categories C_{base} . For novel categories C_{novel} , this hallucinator creates additional features in the RoI head based on the observed feature and the learned parameters. Therefore, the features in the RoI head f^R of novel category samples are augmented by leveraging the shared within-class feature variation from base categories C_{base} . The set of augmented features in the RoI head is used as additional training examples for novel categories C_{novel} .

Sun *et al.* [80] (FSCE) describe the similarity between the augmentation with several random image crops and multiple RoI proposals from the RPN. Thus, increasing the number of proposed RoIs per novel category instance as described in Sec. VII-A is also increasing the variance of novel categories as it resembles random cropping augmentation.

According to [84], increasing the variance of novel categories primarily benefits the extreme few-shot scenario with very few samples K per novel category.

Takeaway: Increasing the variance of training examples from novel categories – e.g. by data augmentation – improves detection accuracy, especially when the number of training examples K is very low.

D. Transfer Knowledge Between Base and Novel Categories

To improve the generalization of low-shot learning in the target domain, in LSTD [8], base category knowledge is transferred to novel-categories before the second training phase. To achieve this, the weights of components for novel classes are initialized by base classes weights using a soft assignment of similar base classes. Only the final classification layer needs to be initialized with random weights for the base classes. The subsequent finetuning is supported by transfer-knowledge regularization as additional loss term (see Sec. VII-F).

Chen *et al.* [94] (AttFDNet) initialize the parameters of the novel object detector using parameters from the base object detector and an imprinting initialization method [95], [96]. Also Li *et al.* [89] (CGDP+FSCN) use imprinting for initialization [95].

By learning and leveraging visual and semantic lingual similarities between the novel and base categories, in the second training phase, Khandelwal *et al.* [91] (UniT) transfer weights for bounding box regression and classification from base categories to novel categories.

Zhu *et al.* [92] (SRR-FSD) represent each category concept by a semantic word embedding learned from a large corpus of text. The detector is trained to project the image representations of objects into this embedding space. In consequence, novel categories are learned from both the visual information and the semantic relation.

Cao *et al.* [90] (FADI) also incorporate the categories' semantic meaning: After training on \mathcal{D}_{base} , they measure the semantic similarity of base and novel categories via WordNet [97]. The authors argue, that in the second finetuning phase, associating novel categories to multiple base categories leads to scattered intra-class structures for the novel categories. Thus, each novel category is associated to exactly one base category with the highest similarity. Afterwards, each novel category is assigned a pseudo label of the associated base category. Then, the whole network is frozen – except for the second fully connected layer in RoI Head – and the network is trained such that it learns to align the feature distribution of the novel category to the associated base category. This leads to low intra-class variation of the novel category but inevitably to confusion between C_{base} and C_{novel} . Thus, in a subsequent discrimination step, the classification branches for C_{base} and C_{novel} are disentangled to learn a good discrimination.

Takeaway: For initializing weights of components for novel categories, knowledge from the semantically most similar base categories should be transferred.

E. Keep the Performance on Base Categories

Many approaches suffer from catastrophic forgetting when trained on C_{novel} . Although the model can be trained on C_{base} as well in the finetuning phase, the performance still drops compared to before finetuning.

Therefore, Fan *et al.* [82] (Retentive R-CNN) propose to use a re-detector with two classification heads for bounding box classification: One head is identical to the first training phase head that is trained only on \mathcal{D}_{base} . This head stays unchanged in the second phase. It is responsible for predicting

objects of \mathcal{C}_{base} . As in TFA [79], the weights of the second head are finetuned on $\mathcal{D}_{base} \cup \mathcal{D}_{novel}$ since training on \mathcal{D}_{novel} only would decrease the generalization due to limited data. During finetuning, a cosine classifier is used to balance the variations in feature norms of \mathcal{C}_{base} and \mathcal{C}_{novel} . The finetuned second head is responsible for predicting objects of \mathcal{C}_{novel} . Additionally, they propose to use a bias-balanced RPN in the second phase that proposes RoIs based on the pretrained RPN and a finetuned RPN, where the weights of the pretrained RPN are frozen to keep the performance on the base categories \mathcal{C}_{base} .

Takeaway: To prevent catastrophic forgetting and keep the performance on base categories, separate heads can be utilized for detecting \mathcal{C}_{novel} and \mathcal{C}_{base} .

F. Modify the Loss Function

A modified loss can guide the detector towards focusing on foreground regions or specific aspects and may also help in improving the consistency in multiple branches. Furthermore, a modification of the loss function can help to control the gradient flow in the detector and to improve the inner- and inter-class variance of features for object classification.

Chen *et al.* [8] (LSTD) use additional background-depression and transfer-knowledge regularization terms in the loss function. Background depression penalizes activations in background regions by ℓ^2 regularization. Thus, the detector focuses more on target objects. The transfer-knowledge regularization helps to incorporate the source-domain knowledge into the training procedure of target-domain.

Li *et al.* [89] (CGDP+FSCN) identified unlabeled instances of novel categories \mathcal{C}_{novel} in the base dataset \mathcal{D}_{base} as problematic. They introduce an additional semi-supervised loss term to also utilize these unlabeled instances. Since this loss also proposes many hard negatives of base categories, they additionally prune the dataset to select only the most likely unlabeled novel category objects.

Chen *et al.* [94] (AttFDNet) propose an object concentration loss to improve the intra-class agreements and a background concentration loss to tackle the problem of unlabeled instances in the dataset. The object concentration loss maximizes the cosine similarity between instances of the same category. The background concentration loss minimizes the cosine similarity between features corresponding to unlabeled instances and the weights for background in the classification layer.

Similar to the meta-learning approach TIP [42], Wu *et al.* [87] (FSOD-UP) use a consistency loss to force features of two branches to be similar. They apply the KL-Divergence loss between these features.

The detector of MPSR [85] contains two branches that are loosely coupled via shared weights. Therefore both branches must contribute to the loss functions of the shared components in the two branches. The magnitude of contribution from each branch is controlled by a scaling parameter. CME [44] builds on top of MPSR, but introduces an additional adversarial training as we described in subsection V-E.

Also Xu *et al.* [93] (FSSP) introduce an auxiliary branch. In their version, it included a full replication of the detection

network with shared weights, an identical processing pipeline, and additional augmentation of objects. A modified classification loss combines the decisions in the original branch and this auxiliary branch that processes only one object with most of the background removed. According to Xu *et al.* [93], this leads to a greater focus on hard samples and consequently to improved detection scores.

Sun *et al.* [80] (FSCE) introduce a new branch in the RoI head. In addition to the standard RoI head they apply a single fully connected layer as contrastive branch to be able to measure similarity scores between learned object proposal representations. On the contrastive branch, they use a contrastive proposal encoding loss for training that enables increasing the cosine similarity of representation from the same category and reduce the similarity of proposals from different categories.

Qiao *et al.* [88] (DeFRCN) additionally want to update the backbone in both training phases, but they identified contradictions in training as problematic. The goals of RPN and ROI head are contrary since the RPN tries to learn class-agnostic region proposals whereas the ROI head tries to distinguish categories. Their extensive experiments showed that it is key to stop the gradient flow from the RPN to the backbone and scale the gradient from the ROI head to the backbone. During training on \mathcal{D}_{base} in the first phase, they scale the gradient from the ROI head by 0.75, so that the backbone learns a little less than the rest of the detector. During training on $\mathcal{D}_{base} \cup \mathcal{D}_{novel}$ in the second phase, it proved necessary to scale the gradient by 0.01, which is in the direction of freezing the backbone. Stopping the gradient from the RPN and scaling the gradient from the ROI head significantly boosts the performance, especially in the second phase. The authors observed, that this gradient scaling also benefits Faster R-CNN as generic object detector, when trained with sufficient data as well.

Cao *et al.* [90] (FADI) introduce an additional set-specialized margin loss to enlarge inter-class separability. In contrast to previous margin losses such as ArcFace [98], they use scaling factors for different margins, where the scaling factor for \mathcal{C}_{novel} is higher than for \mathcal{D}_{base} , as novel categories are much more challenging.

Takeaway: The loss should be modified regarding optimized gradient flow and inter-class separability. In an auxiliary branch, a contrastive loss can help to improve the discriminative power of features, like in two-branch meta learning.

G. Use Attention

Attention blocks help to enhance features. In this sense, Wu *et al.* [87] (FSOD-UP) use soft attention between learned prototypes (see subsection VII-H) and RPN outputs to enhance features in an extra branch.

Yang *et al.* [83] (CoTrans) include an explicit context module into their one-stage detector to integrate contextual information into the representations of objects: First, for each anchor box, by dot product they compare its representation, which is the logit vector in the classification head, with their contextual field, which is constructed by spatially pooled

anchor boxes. Then, Yang *et al.* [83] use the affinity between an anchor box and its contextual field as a relational attention to integrate contexts into the representation of the anchor box.

Xu *et al.* [93] (FSSP) first process the image by a self-attention module and then process the attention-enriched input by a one-stage detector. Therefore, the detector can focus on important parts of the input image.

Chen *et al.* [94] (AttFDNet) combine top-down and bottom-up attention. Top-down attention is learned in supervised fashion in a simplified non-local block and a squeeze-and-excitation block. Bottom-up attention is computed by a saliency prediction model (BMS [99] or SAM [100]).

H. Modify Architecture by an Additional Branch

The majority of transfer learning approaches are based on the Faster R-CNN detector as shown in Fig. 8. Benchmark results confirm the superiority of this two-stage detector for transfer learning approaches. Only few approaches deviate from this architecture.

Li *et al.* [89] (CGDP+FSCN) observed that the performance degradation for novel categories in Faster R-CNN is mainly caused by false positive classifications, i.e., by category confusion. Therefore, they refine the classification in an additional discriminability enhancement branch. This branch is designed as a translation-invariant classifier to produce category-discriminative classification results. To ensure translation-invariance, it intentionally does not share any parameters with the base detector. It directly processes the cropped image of the object to be classified. Then, the classifications of the original Faster R-CNN branch and the refinement branch are fused. To improve the semantic discriminability of the refinement branch, Li *et al.* [89] train it by sampling misclassified false positives from the standard classification branch. Qiao *et al.* [88] (DeFRCN) also observed many low classification scores for novel categories. As Li *et al.*, they conclude that contrary requirements of translation invariant features for classification and translation covariant features for localization are problematic. To tackle this issue, they propose a prototypical calibration block, which performs score refinement to eliminate high-scored false positive classifications.

Wu *et al.* [85] (MPSR) propose to use an auxiliary refinement branch during training that is only loosely coupled with the original branch of the Faster R-CNN via shared weights of the RPN and the RoI head and both branches contributing to the loss functions of the shared components. When the training is finished, the refinement branch is not needed anymore and, therefore, is dropped. This saves computation time during inference.

Wu *et al.* [86] (SVD) build upon MPSR [85]. With a singular value decomposition (SVD), they decompose the backbone features f^B into eigenvectors with their relevance quantified by the corresponding singular values. The eigenvectors corresponding to the largest singular values are able to suppress certain variations (e.g., of style or texture) and are therefore used to enhance the generalization space which is used for localization. In contrast, the eigenvectors corresponding to the smaller singular values may encode more category-related

information (e.g., the structure of objects) and are hence used to build a discrimination space. This discrimination space is further refined by utilizing dictionary learning [101] to facilitate classification.

Wu *et al.* [87] (FSOD-UP) adapt the idea from few-shot learning of learning prototypes [11], [102], [103] that reflect category information. They observed, that category-specific prototypes as used in few-shot learning represent image-level information and fail to capture object characteristics for localizing and recognizing objects. Therefore, they learn universal prototypes based on all categories in an extra branch that takes features from the backbone representing image-level information. These universal prototypes capture intrinsic object characteristics that are invariant under different visual changes and shall help to enhance the original features from the backbone. The original and enhanced features are then concatenated and processed by the RPN. After the RPN, Wu *et al.* further enhance the features with conditional prototypes in another branch. Conditional prototypes are learned similar to universal prototypes, but from features that are outputted from the RPN and, therefore, contain mainly object information. Again, these further enhanced features are concatenated with the original features, and then processed by the ROI head.

In the following, we describe approaches which build upon one-stage detectors: One of the earliest few-shot object detection approaches, LSDT [8], used an architecture that incorporates concepts of SSD [17] and Faster R-CNN [25]. Bounding box regression follows the SSD approach. Chen *et al.* [8] argue that the SSD approach fits very well for localizing objects of various sizes. For object classification, they follow the Faster R-CNN approach, except they use two convolutional layers on top of RoI pooling instead of a fully connected layer for object classification.

Yang *et al.* [83] (CoTrans) use SSD [17] as a one-stage detector. They argue that the multi-scale spatial receptive fields in this architecture provide rich contexts, which are important for knowledge transfer. Chen *et al.* [94] (AttFDNet) also use the SSD detector, but add two attention branches, to help the detector to focus on the important parts of the image, and six prediction heads that predict bounding boxes and categories for objects at different scales.

Xu *et al.* [93] (FSSP) show, how a fast one-stage detector, namely YOLOv3 [20], can be made competitive with the slower two-stage detector Faster R-CNN in the vanilla setup as described in [79]. This is possible only by putting in a lot of effort, namely incorporating a self-attention module, using an additional auxiliary branch that contains a full replication of the detection network, augmenting the input data of the auxiliary branch, and applying an additional loss. However, due to these modifications, the fast one-stage detector of Xu *et al.* [93] is especially performing better than TFA [79] for the extremely low-shot scenario.

Takeaway: In detectors based on Faster R-CNN, a refinement branch can help to reduce false positive classifications. Learning prototypes in an auxiliary branch is also a promising direction. Single-stage detectors can also profit from an auxiliary branch in order to enable data augmentation.

Conclusion on Transfer Learning Approaches

Transfer learning approaches have a much simpler training pipeline, as they do not require complex episodic training as in meta learning. By incorporating specific techniques – such as freezing the correct parts of the network, transferring knowledge between base and novel categories, or modifying the loss function – transfer learning approaches are able reach state of the art performance.

VIII. DATASETS, EVALUATION PROTOCOLS, AND BENCHMARK RESULTS

Evaluation of few-shot object detectors requires tailored datasets that distinguish between base and novel categories. Therefore, most approaches use specific splits of the common object detection datasets PASCAL VOC [104] and Microsoft COCO [105]. Generally, few-shot object detectors are evaluated in the K -shot- N -way manner, i.e., \mathcal{D}_{novel} consists of K labeled examples for N novel categories.

A. PASCAL VOC Dataset

The PASCAL VOC dataset [104] contains annotations for 20 categories. Commonly, the combination of VOC07+12

trainval sets is used for training, and VOC07 test set for testing. For evaluating few-shot object detectors, most often three category splits are used; each with 15 base categories and five novel categories ($N = 5$):

- Set 1: $C_{novel} = \{bird, bus, cow, motorbike, sofa\}$
- Set 2: $C_{novel} = \{aeroplane, bottle, cow, horse, sofa\}$
- Set 3: $C_{novel} = \{boat, cat, motorbike, sheep, sofa\}$

The number of shots K for novel categories is set to 1, 2, 3, 5, and 10. As evaluation metric, the mean average precision at an intersection over union (IoU) threshold of 0.5 is used (AP_{50}). Unfortunately, the specific K -shot object instances are not fixed, which leads to varying instances used in different approaches. As stated by Wang *et al.* [79], this high variance in training samples makes it difficult to compare approaches against each other, as approach-based performance differences may be insignificant compared to differences based on different instances. Therefore, Wang *et al.* [79] propose a revised evaluation protocol, where results are averaged over 30 runs with different random samples of training shots. Moreover, they also report the performance on base categories since ignoring the performance for base categories might hide a potential performance drop and is, therefore, not suitable for

				Novel	Novel Set 1					Novel Set 2					Novel Set 3					Base Set 1	
Approach	Publication	avg. Detector	ft.	mean	K=1	2	3	5	10	1	2	3	5	10	1	2	3	5	10	3	10
▷ AttFDNet (BU+TD) [94]	arXiv 2020	✗ SSD VGG-16	✓	26.9	29.6	34.9	35.1	—	—	16.0	20.7	22.1	—	—	22.6	29.1	32.0	—	—	★	—
• PNPDet [75]	WACV 2021	✗ CenterNet	✓	27.6	18.2	—	27.3	—	41.0	16.6	—	26.5	—	36.4	18.9	—	27.2	—	36.2	75.5	75.5
• MetaYOLO [43]	ICCV 2019	✗ YOLOv2	✓	28.4	14.8	15.5	26.7	33.9	47.2	15.7	15.3	22.7	30.1	40.5	21.3	25.6	28.4	42.8	45.9	64.8	69.7
• Meta Faster-RCNN [52]	arXiv 2021	✗ Faster R-CNN R-101	✗	29.9	36.7	26.2	30.4	35.4	39.1	25.1	22.9	29.0	23.5	25.0	31.1	25.8	31.9	32.5	34.1	—	—
• RepMet [74]	CVPR 2019	✗ Faster R-CNN R-101	✗	30.8	26.1	32.9	34.4	38.6	41.3	17.2	22.1	23.4	28.3	35.8	27.5	31.1	31.5	34.4	37.2	—	—
• MetaDet [76]	ICCV 2019	✓ Faster R-CNN VGG-16	✓	31.0	18.9	20.6	30.2	36.8	49.6	21.8	23.1	27.8	31.7	43.0	20.6	23.9	29.4	43.9	44.1	—	—
• ▷ CME (MetaYOLO) [44]	CVPR 2021	✗ YOLOv2	✓	31.1	17.8	26.1	31.5	44.8	47.5	12.7	17.4	27.1	33.7	40.0	15.7	27.4	30.7	44.9	48.8	—	—
• Meta R-CNN [9]	ICCV 2019	✗ Faster R-CNN R-101	✓	31.1	19.9	25.5	35.0	45.7	51.5	10.4	19.4	29.6	34.8	45.4	14.3	18.2	27.5	41.2	48.1	64.8	67.9
▷ TFA w/cos [79]	ICML 2020	✓ Faster R-CNN R-101	✓	34.7	25.3	36.4	42.1	47.9	52.8	18.3	27.5	30.9	34.1	39.5	17.9	27.2	34.3	40.8	45.6	77.3	77.5
• FSDeView [41]	ECCV 2020	✓ Faster R-CNN R-101	✓	36.7	24.2	35.3	42.2	49.1	57.4	21.6	24.6	31.9	37.0	45.7	21.2	30.0	37.2	43.8	49.6	—	—
• QA-FewDet [54]	ICCV 2021	✓ Faster R-CNN R-101	✗	37.0	41.0	33.2	35.3	47.5	52.0	23.5	29.4	37.9	35.9	37.1	33.2	29.4	37.6	39.8	41.5	—	—
• TIP [42]	CVPR 2021	✓ Faster R-CNN R-101	✓	38.5	27.7	36.5	43.3	50.2	59.6	22.7	30.1	33.8	40.9	46.9	21.7	30.6	38.1	44.5	50.9	—	—
• FSOD-KT [56]	SMC 2020	✗ Faster R-CNN R-101	✓	38.8	27.8	41.4	46.2	55.2	56.8	19.8	27.9	38.7	38.9	41.5	29.5	30.6	38.6	43.8	45.7	69.6	68.1
• DCNet [55]	CVPR 2021	✓ Faster R-CNN R-101	✓	39.2	33.9	37.4	43.7	51.1	59.6	23.2	24.8	30.6	36.7	46.6	32.3	34.9	39.7	42.6	50.7	—	—
▷ TFA w/cos [79]	ICML 2020	✗ Faster R-CNN R-101	✓	39.9	39.8	36.1	44.7	55.7	56.0	23.5	26.9	34.1	35.1	39.1	30.8	34.8	42.8	49.5	49.8	79.1	78.4
▷ Halluc. (TFA) [84]	CVPR 2021	✗ Faster R-CNN R-101	✓	40.6	45.1	44.0	44.7	55.0	55.9	23.2	27.5	35.1	34.9	39.0	30.5	35.1	41.4	49.0	49.3	—	—
▷ Retentive R-CNN [82]	CVPR 2021	✗ Faster R-CNN R-101	✓	41.1	42.4	45.8	45.9	53.7	56.1	21.7	27.8	35.2	37.0	40.3	30.2	37.6	43.0	49.7	50.1	★	★
▷ FSCE [80]	CVPR 2021	✓ Faster R-CNN R-101	✓	41.2	32.9	44.0	46.8	52.9	59.7	23.7	30.6	38.4	43.0	48.5	22.6	33.4	39.5	47.3	54.0	74.1	—
▷ CoRPN w/ cos [81]	arXiv 2020	✗ Faster R-CNN R-101	✓	42.2	44.4	38.5	46.4	54.1	55.7	25.7	29.5	37.3	36.2	41.3	35.8	41.8	44.6	51.6	49.6	—	—
• NP-RepMet [74]	NeurIPS 2020	✗ Faster R-CNN R-101	✗	42.6	37.8	40.3	41.7	47.3	49.4	41.6	43.0	43.4	47.4	49.1	33.3	38.0	39.8	41.5	44.8	66.6	68.3
▷ SRR-FSD (red. pretr.) [92]	CVPR 2021	✗ Faster R-CNN R-101	✓	43.0	46.3	51.1	52.6	56.2	57.3	31.0	29.9	34.7	37.3	41.7	39.2	40.5	39.7	42.2	45.2	—	—
▷ Halluc. (CoRPN) [84]	CVPR 2021	✗ Faster R-CNN R-101	✓	43.2	47.0	44.9	46.5	54.7	54.7	26.3	31.8	37.4	37.4	41.2	40.4	42.1	43.3	51.4	49.6	—	—
▷ CGDP+FSN [89]	CVPR 2021	✗ Faster R-CNN R-50	✓	43.8	40.7	45.1	46.5	57.4	62.4	27.3	31.4	40.8	42.7	46.3	31.2	36.4	43.7	50.1	55.6	—	—
• ▷ CME (MPSR) [44]	CVPR 2021	✗ Faster R-CNN R-101	✓	44.4	41.5	47.5	50.4	58.2	60.9	27.2	30.2	41.4	42.5	46.8	34.3	39.6	45.1	48.3	51.5	—	—
▷ MPSR [85]	ECCV 2020	✗ Faster R-CNN R-101	✓	44.8	41.7	—	51.4	55.2	61.8	24.4	—	39.2	39.9	47.8	35.6	—	42.3	48.0	49.7	67.8	71.8
▷ SRR-FSD [92]	CVPR 2021	✗ Faster R-CNN R-101	✓	44.8	47.8	50.5	51.3	55.2	56.8	32.5	35.3	39.1	40.8	43.8	40.1	41.5	44.3	46.9	46.4	78.2	78.2
• GenDet [45]	TNNLS 2021	✓ Faster R-CNN R-50	✓	44.9	38.5	47.1	52.2	57.7	63.5	26.8	34.0	37.3	42.8	48.3	33.4	40.0	44.3	51.2	56.5	68.4	69.3
▷ SVD (MPSR) [86]	NeurIPS 2021	✗ Faster R-CNN R-101	✓	44.9	41.5	47.4	51.5	57.7	61.2	29.4	29.6	39.8	41.2	51.5	36.0	39.4	45.4	50.4	51.3	69.4	—
▷ FSOD-UP [87]	ICCV 2021	✗ Faster R-CNN R-101	✓	45.0	43.8	47.8	50.3	55.4	61.7	31.2	30.5	41.2	42.2	48.3	35.5	39.7	43.9	50.6	53.5	★	★
▷ FSPP [93]	Access 2021	✗ YOLOv3-SPP	✓	45.1	41.6	—	49.1	54.2	56.5	30.5	—	39.5	41.4	45.1	36.7	—	45.3	49.4	51.3	73.5	74.2
• Meta-DETR [57]	arXiv 2021	✓ Def. DETR R-101	✓	45.8	35.1	49.0	53.2	57.4	62.0	27.9	32.3	38.4	43.2	51.8	34.9	41.8	47.1	54.1	58.2	70.0	73.5
• Meta Faster-RCNN [52]	arXiv 2021	✗ Faster R-CNN R-101	✓	46.2	41.8	46.7	52.7	59.6	62.3	26.1	33.6	43.8	47.8	50.1	35.6	42.1	45.8	53.4	52.3	—	—
▷ FSCE [80]	CVPR 2021	✗ Faster R-CNN R-101	✓	46.6	44.2	43.8	51.4	61.9	63.4	27.3	29.5	43.5	44.2	50.2	37.2	41.9	47.5	54.6	58.5	74.1	—
▷ SVD (FSCE) [86]	NeurIPS 2021	✗ Faster R-CNN R-101	✓	46.7	46.1	43.5	48.9	60.0	61.7	25.6	29.9	44.8	47.5	48.2	39.5	45.4	48.9	53.9	56.9	74.8	—
• MM-FSOD [46]	arXiv 2020	✓ Faster R-CNN R-34	✗	47.6	50.0	—	55.9	57.9	60.9	37.3	—	45.7	46.5	48.2	35.6	—	43.3	44.1	45.4	—	—
• SQMG [39]	CVPR 2021	✗ Faster R-CNN R-50	✗	47.7	46.8	49.2	50.2	52.0	52.4	39.4	43.1	43.6	44.1	45.7	44.1	49.8	50.5	52.3	52.8	—	—
• QA-FewDet [54]	ICCV 2021	✓ Faster R-CNN R-101	✓	48.0	42.4	51.9	55.7	62.6	63.4	25.9	37.8	46.6	48.9	51.1	35.2	42.9	47.8	54.8	53.5	—	—
▷ FADI [90]	NeurIPS 2021	✗ Faster R-CNN R-101	✓	49.2	50.3	54.8	54.2	59.3	63.2	30.6	35.0	40.3	42.8	48.0	45.7	49.7	49.1	55.0	59.6	78.9	—
▷ DeFRCN (base+novel) [88]	ICCV 2021	✓ Faster R-CNN R-101	✓	49.4	40.2	53.6	58.2	63.6	66.5	29.5	39.7	43.4	48.1	52.8	35.0	38.3	52.9	57.7	60.8	★	★
• SQMG [39]	CVPR 2021	✗ Faster R-CNN R-101	✗	49.8	48.6	51.1	52.0	53.7	54.3	41.6	45.4	45.8	46.3	48.0	46.1	51.7	52.6	54.1	55.0	—	—
• Meta-RetinaNet [77]	BMVC 2020	✗ RetinaNet ResNet18	✓	49.9	38.3	51.8	59.3	65.3	71.5	28.4	36.8	42.4	45.5	50.9	35.9	48.1	53.2	58.0	63.6	—	—
• Meta-DETR [57]	arXiv 2021	✓ Def. DETR R-101	✓	50.2	40.6	51.4	58.0	59.2	63.6	37.0	36.6	43.7	49.1	54.6	41.6	45.9	52.7	58.9	60.6	70.0	73.5
▷ DeFRCN (just novel) [88]	ICCV 2021	✓ Faster R-CNN R-101	✓	51.9	53.6	57.5	61.5	64.1	60.8	30.1	38.1	47.0	53.3	47.9	48.4	50.9	52.3	54.9	57.4	—	—
▷ UniT * [91]	CVPR 2021	✗ Faster R-CNN R-101	✓	67.8	75.7	75.8	75.9	76.1	76.7	57.2	57.4	57.9	58.2	63.0	67.6	68.1	68.2	68.6	70.0	77.8	77.7

TABLE I: AP_{50} published results on the PASCAL VOC benchmark for all three sets and different number of shots K . We sort the approaches by the average over all novel sets and shots. avg.: averaged over multiple runs. ft.: finetuned on \mathcal{D}_{novel} . —: no result reported in paper. ★: results only reported for different shots or sets, therefore these results are not included here. *: Results for UniT [91] are provided with additional image-level supervision, therefore a fair comparison to other approaches is not possible. †: dual-branch meta learning. •: single-branch meta learning. ▷: transfer learning.

evaluating the overall performance of a model.

In Tab. I, we list benchmark results of the described approaches for the PASCAL VOC dataset. Additionally, we characterize each approach. As we can see, most approaches utilize a Faster R-CNN [25] detector with ResNet-101 [26] as backbone. Furthermore, we report whether the results are averaged over multiple runs as proposed by Wang *et al.* [79], as otherwise results for a single run might be cherry-picked. In general, both transfer learning and dual-branch meta learning approaches can achieve similar results.

The best results are achieved by the transfer learning approach UniT, which, however, additionally receives image-level supervision and, thus, follows an easier evaluation protocol. Within all other approaches, which do not use this additional information, DeFCRN [88] and Meta-DETR [57] perform best. The transfer learning approach DeFCRN modifies the loss function for the detector’s backbone to control the gradient flow from the RPN and ROI head to the backbone. Therefore, in DeFCRN the backbone can be finetuned during the second training phase on \mathcal{D}_{novel} as well. Moreover, in DeFCRN an additional branch is used for score refinement to reduce false positive classifications. The dual-branch meta learning approach Meta-DETR [57] excels by utilizing a transformer-based architecture with attention mechanisms. For Meta-DETR the performance on base categories was reported as well. DeFCRN also provides results after finetuning on both novel and base categories, which however impedes performance on novel categories.

Some meta learning approaches can simply be applied to \mathcal{D}_{novel} without requiring finetuning. Here, the best approaches are SQMG [39] and MM-FSOD [46]. Both apply several concepts for improving the performance, as shown in Fig. 4: They increase the discriminative power of support features, aggregate several support images in an advanced manner, and use a category-agnostic bounding box computation. SQMG additionally aggregates features before the RPN and incorporates spatial information into aggregation.

Although it is very commonly used, according to Michaelis *et al.* [51], the PASCAL VOC dataset is too easy: With a dual-branch meta learning approach and uninformative

all-black support images, they are still able to locate the novel objects and reach a mAP_{50} of 33.2. However, we want to highlight that in general objects do not simply need to be *located* but also *classified*, i.e., detectors need to also determine which category is present in the image.

B. Microsoft COCO Dataset

In comparison to PASCAL VOC, the Microsoft COCO dataset [105] is more challenging and contains annotations for 80 categories, including the 20 VOC categories. For few-shot object detection, most often the 20 VOC categories are used as novel categories, leaving the remaining 60 categories as base categories. Typically, the number of shots K is set to 10 and 30. However, some approaches focus on the extremely low-shot regime and use only 1–3 shots per category.

For evaluation, the standard COCO metrics are used: The primary metric is $AP_{50:95}$: the mean of 10 average precision values with IoU thresholds in range $[0.5, 0.95]$. Moreover, AP_{50} is reported, which corresponds to the Pascal VOC metric. AP_{75} is more strict, as detections only count as positive when their IoU with a ground truth object is larger than 0.75. Some approaches also report average recall AR_1 , AR_{100} and AR_{1000} for 1, 100 or 1000 detections per image, respectively. Average precision and average recall are also available for small, medium-sized and large objects (AP_S , AP_M , AP_L , AR_S , AR_M , AR_L).

We list published benchmark results for $K = 10$ in Tab. III and $K = 30$ in Tab. V. Results for the extreme 1-shot scenario are shown in Tab. II. Similar to PASCAL VOC, the evaluation of few-shot detectors on Microsoft COCO also suffers from varying K -shot instances between approaches. Therefore, in the tables we denote whether the revised evaluation protocol proposed by Wang *et al.* [79] was used (column avg.), where results over 10 runs with different random samples are averaged.

Also for the Microsoft COCO dataset, UniT [91] achieves the highest performance, but has access to image-level annotations during evaluation, which prevents a fair comparison. DANa [47] seems also to perform very well, but uses a 1-way evaluation setting which requires the detector to only

Approach	Publication	avg.	Detector	ft.	Novel Categories			Base Categories		
					AP	AP50	AP75	AP	AP50	AP75
▷ TFA w/cos [79]	ICML 2020	✓	Faster R-CNN R-101	✓	1.9	3.8	1.7	31.9	51.8	34.3
▷ CoRPN w/ cos [81]	arXiv 2020	✗	Faster R-CNN R-50	✓	3.7	6.8	3.8	32.1	52.9	34.4
▷ Halluc. (TFA w/cos) [84]	CVPR 2021	✗	Faster R-CNN R-101	✓	3.8	6.5	4.3	31.5	50.8	33.9
▷ CoRPN w/ cos [81]	arXiv 2020	✗	Faster R-CNN R-101	✓	4.1	7.2	4.4	34.1	55.1	36.5
▷ Halluc. (CoRPN w/cos) [84]	CVPR 2021	✗	Faster R-CNN R-101	✓	4.4	7.5	4.9	32.3	52.4	34.4
• Meta Faster-RCNN [52]	arXiv 2021	✗	Faster R-CNN R-101	✓	4.8	10.0	4.4	—	—	—
▷ DeFCRN [88]	ICCV 2021	✓	Faster R-CNN R-101	✓	4.8	—	—	—	—	—
• QA-FewDet [54]	ICCV 2021	✓	Faster R-CNN R-101	✓	4.9	10.3	4.4	—	—	—
• Meta Faster-RCNN [52]	arXiv 2021	✗	Faster R-CNN R-101	✗	5.0	10.2	4.6	—	—	—
• QA-FewDet [54]	ICCV 2021	✓	Faster R-CNN R-101	✗	5.1	10.5	4.5	—	—	—
▷ FADI [90]	NeurIPS 2021	✗	Faster R-CNN R-101	✓	5.7	10.4	6.0	—	—	—
• Meta-DETR [57]	arXiv 2021	✓	Deformable DETR R-101	✓	7.5	12.5	7.7	—	—	—
▷ DeFCRN [88]	ICCV 2021	✗	Faster R-CNN R-101	✓	9.3	—	—	—	—	—
• DANa * [47]	TMM 2021	✗	Faster R-CNN R-50	✗	11.9	25.6	10.4	27.8	46.3	27.7

TABLE II: Benchmark results on the 1-shot Microsoft COCO dataset sorted by novel AP. avg.: averaged over multiple runs. ft.: finetuned on \mathcal{D}_{novel} . *: DANa [47] uses the easier 1-way evaluation protocol, which prevents a fair comparison. —: no result reported in paper. •: dual-branch meta learning. •: single-branch meta learning. ▷: transfer learning.

Approach	Publication	avg.	Detector	ft.	Novel Categories												Base Cat.	
					Average Precision						Average Recall						AP	AR
					50-95	50	75	S	M	L	1	10	100	S	M	L	50-95	1
• ONCE [58]	CVPR 2020	✗	CentreNet R-50	✗	5.1	—	—	—	—	—	—	—	—	—	—	—	22.9	29.9
• PNPDet [75]	WACV 2021	✗	CenterNet DLA-34 Def.	✓	5.5	—	—	—	—	—	12.6	—	—	—	—	—	25.8	25.5
• MetaYOLO [43]	ICCV 2019	✗	YOLOv2	✓	5.6	12.3	4.6	0.9	3.5	10.5	10.1	14.3	14.4	1.5	8.4	28.2	—	—
• Meta Faster-RCNN [52]	arXiv 2021	✗	Faster R-CNN R-50	✗	7.0	14.7	5.9	—	—	—	—	—	—	—	—	—	29.1	—
• Meta Faster-RCNN [52]	arXiv 2021	✗	Faster R-CNN R-50	✓	7.0	15.3	5.7	—	—	—	—	—	—	—	—	—	29.1	—
• MetaDet [76]	ICCV 2019	✓	Faster R-CNN VGG-16	✓	7.1	14.6	6.1	1.0	4.1	12.2	11.9	15.1	15.5	1.7	9.7	30.1	—	—
• MM-FSOD [46]	arXiv 2020	✓	Faster R-CNN R-34	✗	8.2	19.2	8.0	—	—	—	—	—	—	—	—	—	—	—
• Meta R-CNN [9]	ICCV 2019	✗	Faster R-CNN R-101	✓	8.7	19.1	6.6	2.3	7.7	14.0	12.6	17.8	17.9	7.8	15.6	27.2	—	—
▷ CoRPN w/ cos [81]	arXiv 2020	✗	Faster R-CNN R-50	✓	9.0	17.6	8.3	—	—	—	—	—	—	—	—	—	32.7	—
▷ TFA w/cos [79]	ICML 2020	✓	Faster R-CNN R-101	✓	9.1	—	—	—	—	—	—	—	—	—	—	—	32.4	—
• GenDet [45]	TNNLS 2021	✓	Faster R-CNN R-50	✓	9.2	17.7	8.8	3.3	7.7	14.6	—	—	—	—	—	—	—	—
▷ Meta Faster-RCNN [52]	arXiv 2021	✗	Faster R-CNN R-101	✗	9.3	17.3	8.8	—	—	—	—	—	—	—	—	—	—	—
▷ Retentive R-CNN [82]	CVPR 2021	✓	Faster R-CNN R-101	✓	9.5	—	—	—	—	—	—	—	—	—	—	—	39.2	—
• Meta-RetinaNet [77]	BMVC 2020	✗	RetinaNet R-18	✓	9.7	19.9	7.7	2.8	8.5	15.2	13.4	18.9	19.0	8.3	17.1	32.8	—	—
▷ MPSR [85]	ECCV 2020	✗	Faster R-CNN R-101	✓	9.8	17.9	9.7	3.3	9.2	16.1	15.7	21.2	21.2	4.6	19.6	34.3	—	—
• GenDet [45]	TNNLS 2021	✓	Faster R-CNN R-101	✓	9.9	18.8	9.6	3.6	8.4	15.4	—	—	—	—	—	—	—	—
▷ FSSP [93]	Access 2021	✗	YOLOv3-SPP	✓	9.9	20.4	9.6	—	—	—	—	—	—	—	—	—	—	—
▷ TFA w/cos [79]	ICML 2020	✗	Faster R-CNN R-101	✓	10.0	—	9.3	—	—	—	—	—	—	—	—	—	—	—
• QA-FewDet [54]	ICCV 2021	✓	Faster R-CNN R-101	✗	10.2	20.4	9.0	—	—	—	—	—	—	—	—	—	—	—
▷ Retentive R-CNN [82]	CVPR 2021	✗	Faster R-CNN R-101	✓	10.5	—	—	—	—	—	—	—	—	—	—	—	39.2	—
▷ CoRPN w/ cos [81]	arXiv 2020	✗	Faster R-CNN R-101	✓	10.6	19.9	10.1	—	—	—	—	—	—	—	—	—	34.6	—
▷ FSOD-UP [87]	ICCV 2021	✗	Faster R-CNN R-101	✓	11.0	—	10.7	4.5	11.2	17.3	—	—	—	—	—	—	—	—
▷ SVD (MPSR) [86]	NeurIPS 2021	✗	Faster R-CNN R-101	✓	11.0	—	10.6	4.4	11.5	17.1	—	—	—	—	—	—	—	—
• AttentionRPN [49]	CVPR 2020	✗	Faster R-CNN R-50	✗	11.1	—	—	—	—	—	—	—	—	—	—	—	—	—
▷ FSCE [80]	CVPR 2021	✓	Faster R-CNN R-101	✓	11.1	—	9.8	—	—	—	—	—	—	—	—	—	—	—
▷ SRR-FSD [92]	CVPR 2021	✗	Faster R-CNN R-101	✓	11.3	23.0	9.8	—	—	—	—	—	—	—	—	—	—	—
▷ CGDP+FSFN [89]	CVPR 2021	✗	Faster R-CNN R-50	✓	11.3	20.3	—	—	—	—	—	—	—	—	—	—	—	—
• Meta Faster-RCNN [52]	WACV 2021	✗	Faster R-CNN R-101	✓	11.3	23.5	9.8	—	—	—	—	—	—	—	—	—	—	—
• QA-FewDet [54]	ICCV 2021	✓	Faster R-CNN R-101	✓	11.6	23.9	9.8	—	—	—	—	—	—	—	—	—	—	—
▷ FSCE [80]	CVPR 2021	✗	Faster R-CNN R-101	✓	11.9	—	10.5	—	—	—	—	—	—	—	—	—	—	—
▷ SVD (FSCE) [86]	NeurIPS 2021	✗	Faster R-CNN R-101	✓	12.0	—	10.4	4.2	12.1	18.9	—	—	—	—	—	—	—	—
▷ FADI [90]	NeurIPS 2021	✗	Faster R-CNN R-101	✓	12.2	22.7	11.9	—	—	—	—	—	—	—	—	—	—	—
• FsDetView [41]	ECCV 2020	✓	Faster R-CNN R-50	✓	12.5	27.3	9.8	2.5	13.8	19.9	20.0	25.5	25.7	7.5	27.6	38.9	—	—
• SQMG [39]	CVPR 2021	✗	Faster R-CNN R-50	✗	12.6	27.0	10.9	7.3	13.4	17.8	—	—	—	—	—	—	—	—
• DCNet [55]	CVPR 2021	✓	Faster R-CNN R-101	✓	12.8	23.4	11.2	4.3	13.8	21.0	18.1	26.7	25.6	7.9	24.5	36.7	—	—
▷ AttFDNet (BU+TD) [94]	arXiv 2020	✗	SSD VGG-16	✓	12.9	19.5	13.9	—	—	—	—	—	—	—	—	—	—	—
• SQMG [39]	CVPR 2021	✗	Faster R-CNN R-101	✗	13.9	29.5	11.7	7.6	15.2	19.0	—	—	—	—	—	—	—	—
▷ CME [44]	CVPR 2021	✗	MetaYOLO (YOLOv2)	✓	15.1	24.6	16.4	4.6	16.6	26.0	16.3	22.6	22.8	6.6	24.7	39.7	—	—
• TIP [42]	CVPR 2021	✓	Faster R-CNN R-101	✓	16.3	33.2	14.1	5.4	17.5	25.8	23.6	30.2	30.5	12.7	32.3	43.8	—	—
▷ DeFCRN (base+novel) [88]	ICCV 2021	✓	Faster R-CNN R-101	✓	16.8	—	—	—	—	—	—	—	—	—	—	—	34.0	—
▷ DeFCRN (just novel) [88]	ICCV 2021	✓	Faster R-CNN R-101	✓	18.5	—	—	—	—	—	—	—	—	—	—	—	—	—
• DAnA * [47]	TMM 2021	✗	Faster R-CNN R-50	✓	18.6	—	17.2	—	—	—	—	—	—	—	—	—	—	—
• Meta-DETR [57]	arXiv 2021	✓	Deformable DETR R-101	✓	19.0	30.5	19.7	—	—	—	—	—	—	—	—	—	—	—
▷ UniT * [91]	CVPR 2021	✗	Faster R-CNN R-50	✓	21.7	40.8	20.6	9.1	23.8	31.3	21.1	35.1	36.4	16.5	37.5	51.0	—	—

TABLE III: Benchmark results for 10-shot on the Microsoft COCO dataset sorted by novel $AP_{50:95}$. avg.: averaged over multiple runs. ft.: finetuned on \mathcal{D}_{novel} . *: Deviating evaluation – Results for UniT [91] are provided with image-level supervision and are thus higher; DAnA [47] uses easier 1-way evaluation protocol. —: no result reported in paper. •: dual-branch meta learning. •: single-branch meta learning. ▷: transfer learning.

estimate whether the current query image I^Q contains the object and where it is located, but eliminates the difficulty of correct classification. This also prevents a fair comparison. As in the PASCAL VOC benchmark, among the approaches with a comparable evaluation setting, Meta-DETR [57] and DeFCRN [88] achieve the best results. The best performing approach that does not require finetuning on \mathcal{D}_{novel} is again SQMG [39]. The relative order of the approaches is similar for 1, 10 and 30 shots.

For the extreme case of $K = 1$, it is noticeable that it might be preferable to not finetune on \mathcal{D}_{novel} . This is supported by the results of QA-FewDet [54] and Meta Faster R-CNN [52] that both perform better in case of not finetuning, as can be seen in Tab. II.

C. FSOD Dataset

In contrast to VOC and COCO, the FSOD dataset [49] is specifically designed for few-shot object detection, but

rarely used so far. It is comprised of images from other datasets such as ImageNet [106] and OpenImages [107]. In total, there are 1000 categories of which 800 are used as base categories, and the remaining 200 categories as novel categories. Fan *et al.* [49] constructed the dataset such that the 200 novel categories are the most distinct to the remaining base categories. Moreover, the novel categories do not contain any COCO categories, which allows pretraining with COCO. Despite the many categories, the dataset remains compact, as

Approach	Publication	avg.	Detector	ft.	AP50	AP75
• AttentionRPN [49]	CVPR 2020	✗	Faster R-CNN R-50	✗	27.5	19.4
• MM-FSOD [46]	arXiv 2020	✓	Faster R-CNN R-34	✗	51.7	31.1

TABLE IV: Results for 2-way-5-shot evaluation on the FSOD [49] dataset. avg.: averaged over multiple runs. ft.: finetuned on \mathcal{D}_{novel} .

					Novel Categories												Base Cat.	
Approach	Publication	avg.	Detector	ft.	Average Precision						Average Recall						AP	AR
					50-95	50	75	S	M	L	1	10	100	S	M	L	50-95	1
• MetaYOLO [43]	ICCV 2019	✗	YOLOv2	✓	9.1	19.0	7.6	0.8	4.9	16.8	13.2	17.7	17.8	1.5	10.4	33.5	—	—
• Meta Faster-RCNN [52]	arXiv 2021	✗	Faster R-CNN R-50	✗	10.2	20.5	9.3	—	—	—	—	—	—	—	—	—	29.1	—
• Meta Faster-RCNN [52]	arXiv 2021	✗	Faster R-CNN R-101	✗	10.7	19.6	10.6	—	—	—	—	—	—	—	—	—	—	—
• MetaDet [76]	ICCV 2019	✓	Faster R-CNN VGG-16	✓	11.3	21.7	8.1	1.1	6.2	17.3	14.5	18.9	19.2	1.8	11.1	34.4	—	—
• QA-FewDet [54]	ICCV 2021	✓	Faster R-CNN R-101	✗	11.5	23.4	10.3	—	—	—	—	—	—	—	—	—	—	—
▷ TFA w/cos [79]	ICML 2020	✓	Faster R-CNN R-101	✓	12.1	—	12.0	—	—	—	—	—	—	—	—	—	34.2	—
• Meta R-CNN [9]	ICCV 2019	✗	Faster R-CNN R-101	✓	12.4	25.3	10.8	2.8	11.6	19.0	15.0	21.4	21.7	8.6	20.0	32.1	—	—
▷ Retentive R-CNN [82]	CVPR 2021	✓	Faster R-CNN R-101	✓	12.4	—	—	—	—	—	—	—	—	—	—	—	39.3	—
• Meta-RetinaNet [77]	BMVC 2020	✗	RetinaNet R-18	✓	13.1	26.7	11.2	3.3	13.1	20.2	16.7	22.5	22.8	8.7	21.5	38.7	—	—
▷ CoRPn w/ cos [81]	arXiv 2020	✗	Faster R-CNN R-50	✓	13.4	24.6	13.3	—	—	—	—	—	—	—	—	—	33.5	—
▷ TFA w/cos [79]	ICML 2020	✗	Faster R-CNN R-101	✓	13.7	—	13.4	—	—	—	—	—	—	—	—	—	—	—
▷ Retentive R-CNN [82]	CVPR 2021	✗	Faster R-CNN R-101	✓	13.8	—	—	—	—	—	—	—	—	—	—	—	39.3	—
▷ CoRPn w/ cos [81]	arXiv 2020	✗	Faster R-CNN R-101	✓	13.9	25.1	13.9	—	—	—	—	—	—	—	—	—	35.8	—
• GenDet [45]	TNNLS 2021	✓	Faster R-CNN R-50	✓	14.0	26.7	13.2	4.4	12.1	23.3	—	—	—	—	—	—	—	—
▷ MPSR [85]	ECCV 2020	✗	Faster R-CNN R-101	✓	14.1	25.4	14.2	4.0	12.9	23.0	17.7	24.2	24.3	5.5	21.0	39.3	—	—
▷ FSSP [93]	Access 2021	✗	YOLOv3-SPP	✓	14.2	25.0	13.9	—	—	—	—	—	—	—	—	—	—	—
• GenDet [45]	TNNLS 2021	✓	Faster R-CNN R-101	✓	14.3	27.5	13.8	4.8	13.0	24.2	—	—	—	—	—	—	—	—
• FsDetView [41]	ECCV 2020	✓	Faster R-CNN R-50	✓	14.7	30.6	12.2	3.2	15.2	23.8	22.0	28.2	28.4	8.3	30.3	42.1	—	—
▷ SRR-FSD [92]	CVPR 2021	✗	Faster R-CNN R-101	✓	14.7	29.2	13.5	—	—	—	—	—	—	—	—	—	—	—
▷ CGDP+FSN [89]	CVPR 2021	✗	Faster R-CNN R-50	✓	15.1	29.4	—	—	—	—	—	—	—	—	—	—	—	—
▷ FSCE [80]	CVPR 2021	✓	Faster R-CNN R-101	✓	15.3	—	14.2	—	—	—	—	—	—	—	—	—	—	—
• Meta Faster-RCNN [52]	arXiv 2021	✗	Faster R-CNN R-50	✓	15.4	31.7	13.4	—	—	—	—	—	—	—	—	—	29.1	—
▷ FSOD-UP [87]	ICCV 2021	✗	Faster R-CNN R-101	✓	15.6	—	15.7	4.7	15.1	25.1	—	—	—	—	—	—	—	—
• Meta Faster-RCNN [52]	arXiv 2021	✗	Faster R-CNN R-101	✓	15.9	31.9	14.7	—	—	—	—	—	—	—	—	—	—	—
▷ SVD (FSCE) [86]	NeurIPS 2021	✗	Faster R-CNN R-101	✓	16.0	—	15.3	6.0	16.8	24.9	—	—	—	—	—	—	—	—
▷ FADI [90]	NeurIPS 2021	✗	Faster R-CNN R-101	✓	16.1	29.1	15.8	—	—	—	—	—	—	—	—	—	—	—
▷ SVD (MPSR) [86]	NeurIPS 2021	✗	Faster R-CNN R-101	✓	16.2	—	15.9	4.6	14.6	26.6	—	—	—	—	—	—	—	—
▷ AtFDNet (BU+TD) [94]	arXiv 2020	✗	SSD VGG-16	✓	16.3	24.6	17.3	—	—	—	—	—	—	—	—	—	—	—
▷ FSCE [80]	CVPR 2021	✗	Faster R-CNN R-101	✓	16.4	—	16.2	—	—	—	—	—	—	—	—	—	—	—
• QA-FewDet [54]	ICCV 2021	✓	Faster R-CNN R-101	✓	16.5	31.9	15.5	—	—	—	—	—	—	—	—	—	—	—
▷ CME [44]	CVPR 2021	✗	MetaYOLO (YOLOv2)	✓	16.9	28.0	17.8	4.6	18.0	29.2	17.5	23.8	24.0	6.0	24.6	42.5	—	—
• TIP [42]	CVPR 2021	✓	Faster R-CNN R-101	✓	18.3	35.9	16.9	6.0	19.3	29.2	25.2	32.0	32.3	14.1	34.6	45.1	—	—
• DCNet [55]	CVPR 2021	✓	Faster R-CNN R-101	✓	18.6	32.6	17.5	6.9	16.5	27.4	22.8	27.6	28.6	8.4	25.6	43.4	—	—
▷ DeFRCN (base+novel) [88]	ICCV 2021	✓	Faster R-CNN R-101	✓	21.2	—	—	—	—	—	—	—	—	—	—	—	34.8	—
• DAnA * [47]	TMM 2021	✗	Faster R-CNN R-50	✓	21.6	—	20.3	—	—	—	—	—	—	—	—	—	—	—
• Meta-DETR [57]	arXiv 2021	✗	Deformable DETR R-101	✓	22.2	35.0	22.8	—	—	—	—	—	—	—	—	—	—	—
▷ DeFRCN (just novel) [88]	ICCV 2021	✓	Faster R-CNN R-101	✓	22.6	—	—	—	—	—	—	—	—	—	—	—	—	—
▷ UniT * [91]	CVPR 2021	✗	Faster R-CNN R-50	✓	23.1	43.0	21.6	9.8	25.3	33.8	22.4	36.7	37.9	16.5	38.7	53.3	—	—

TABLE V: Benchmark results for 30-shot on the Microsoft COCO dataset sorted by novel $AP_{50:95}$. avg.: averaged over multiple runs. ft.: finetuned on \mathcal{D}_{novel} . *: Deviating evaluation – Results for UniT [91] are provided with image-level supervision and are thus higher; DANA [47] uses easier 1-way evaluation protocol. —: no result reported in paper. •: dual-branch meta learning. •: single-branch meta learning. ▷: transfer learning.

the most frequent category still has no more than 208 images. With around 66K images, the FSOD dataset contains only about half as many images as the COCO dataset and therefore allows for faster training.

Fan *et al.* [49] propose a 2-way-5-shot evaluation protocol, where models are only pretrained on \mathcal{D}_{base} and not finetuned on \mathcal{D}_{novel} . Counterintuitively, approaches do not need to differentiate between the 200 novel categories. MM-FSOD [46] is so far the only approach reusing the FSOD dataset and achieves higher performance than AttentionRPN [49], as shown in Tab. IV.

D. Other Datasets

Some early approaches for few-shot object detection [8], [73], [74] use the ImageNet-LOC detection dataset. Karlin-sky *et al.* [73] (RepMet) design a benchmark by training on the first 100 categories (mostly animals) and evaluating on 214 unseen animal categories in a 5-way manner.

Despite being rarely used so far, the long-tail LVIS dataset [30] could also be utilized for few-shot object detection: For the LVIS dataset the COCO images were re-annotated with 1203 categories. The categories can be split in

405 frequent (>100 training examples), 461 common (11–100 training examples) and 337 rare (1–10 training examples) categories, containing 71 categories with just one training example. For few-shot object detection, the rare categories with at most 10 training examples can be utilized as novel categories \mathcal{C}_{novel} and the others as base categories \mathcal{C}_{base} . However, it should be noted, that the rare categories are also rare in the validation set and, thus, prone to high variance in evaluation. So far, the LVIS dataset with this split has only been used by TFA [79] and LST [32].

E. Problems of Common Evaluation Protocols

1) High Variance for Different Samples:

As pointed out by Wang *et al.* [79], the use of different samples for novel categories can lead to a high variance in performance and, therefore, makes comparison difficult. Hence, we highly recommend to always report the average of the results over multiple random runs.

2) ImageNet Pretraining and Choice of Novel Categories:

Most methods use an ImageNet-pretrained backbone. While this is common for generic object detection, it has a negative side-effect for few-shot object detection: The novel object categories are not truly novel anymore, as the model has probably already seen images of this category. However, omitting ImageNet pretraining altogether results in worse performance even for the base categories. To alleviate this problem, there are two options:

First, the ImageNet categories which correspond to the novel categories can be excluded from ImageNet-pretraining as done in [50], [92], [48]. CoAE [50] and AIT [48] even remove all COCO-related categories from ImageNet, which results in 275 categories being removed. However, as Zhu *et al.* [92] (SRR-FSD) argue, removing all COCO-related categories is not realistic, as these categories are very common in the natural world and removing 275 categories may affect the representational power learned through pretraining. Therefore, Zhu *et al.* [92] only remove categories corresponding to novel categories for PASCAL VOC, resulting in 50 categories being removed on average. Yet, this requires an additional pretraining for every different set of novel categories.

In Tab. VI, we show results on VOC when pretraining with all 1000 ImageNet categories vs. when reducing the number of categories to 725 in order to remove all COCO-related categories. All these approaches use a different split for base and novel categories than the one described above, with just $N = 4$ novel categories: $\mathcal{C}_{\text{novel}} = \{\text{cow}, \text{sheep}, \text{cat}, \text{aeroplane}\}$. We refer to this as novel set 4. We can see that for CoAE [50] the performance drop is rather high, whereas AIT [48] is able to better handle pretraining with reduced categories.

Approach	Publication	Detector	ImageNet	Novel	Base
• CoAE [50]	NeurIPS 2019	Faster R-CNN R-50	725	63.8	55.1
• CoAE [50]	NeurIPS 2019	Faster R-CNN R-50	1000	68.2	60.1
• AIT [48]	CVPR 2021	Faster R-CNN R-50	725	72.2	67.2
• AIT [48]	CVPR 2021	Faster R-CNN R-50	1000	73.1	69.2

TABLE VI: Effect of removing COCO-related categories from ImageNet to prevent foreseeing novel categories. AP_{50} results on PASCAL VOC novel set 4 are reported. All approaches are one-shot approaches and do not finetune on $\mathcal{D}_{\text{novel}}$.

The second option for preventing foreseeing novel categories is using a dataset with novel categories that do not occur in ImageNet categories. Such a dataset would also be more realistic. Using categories such as cats as novel categories is absurd as there is loads of annotated data. Few-shot object detection aims at detecting objects with only limited annotated instances available. Therefore, a more realistic approach would be to select novel categories that are indeed rare. E.g., the LVIS [30] dataset provides a natural long tail with more and less frequent categories. A maximum of 10 training instances are available for rare categories. Therefore, they can be used as novel categories.

3) One-way Evaluation:

In general, object detection is the joint task of localizing and classifying object instances. However, some few-shot approaches deviate from this setting and create a simpler

task: For example, some approaches that explicitly focus on the one-shot scenario (CoAE [50], AIT [48], OSWF [53] CGG [51]) assume each query image I^Q to have at least one instance of the object category c from the support image $I^{S,c}$. Implicitly, this removes the classification task and only requires localization. The same applies to the 1-way training and evaluation setting of DAnA [47], where the detector only needs to estimate whether the current query image I^Q contains the object and where it is located, but the difficulty of correct classification is eliminated.

In order to report comparable results, we therefore strongly recommend to always evaluate with the N -way setting.

IX. CURRENT TRENDS

As current trends for few-shot object detection, we identified the following: Dual-branch meta learning architectures benefit from transformer-based attention mechanisms for aggregating support and query features. Moreover, transformers will likely replace the current Faster R-CNN backbone, as it is already the case in Meta-DETR [57]. In both dual-branch meta learning and transfer learning approaches, we see the rise of using additional loss functions to create more discriminative features for increasing the inter-class variance and decreasing the inner-class variance. In addition, more and more often a supplementary branch is utilized that receives augmented images in order to increase the low variance of novel object instances. For transfer learning approaches, the current research shows that freezing most of the weights is disadvantageous. Instead, by carefully adjusting the gradient flow, more components can be trained in the second finetuning phase as well, thus achieving higher performance.

Besides these trends in improving few-shot object detection approaches, the extension of few-shot object detection concepts to further research areas such as a weakly-supervised setting or to few-shot instance segmentation is also a current trend. For the weakly-supervised setting, there are only image-level annotations and no bounding boxes, which makes the problem even harder. A first approach towards this direction is StarNet [108]. In contrast, few-shot instance segmentation requires not just bounding boxes but a pixel-level segmentation of the objects, which is already explored by, e.g., FGN [109] and FAPIS [110].

Even though most few-shot object detection approaches are evaluated on the PASCAL VOC and Microsoft COCO datasets currently, we would like to encourage future research to additionally evaluate on more realistic datasets such as LVIS or FSOD, as already done in [49], [46], [79], [32].

X. CONCLUSION

In this survey, we provided an overview of the state of the art for few-shot object detection. We categorized the approaches according to their training scheme and architectural layout into single-branch and dual-branch meta learning and transfer learning. Meta learning approaches use episodic training in the N -way- K -shot setting to improve the subsequent learning with few object instances per novel category. Dual-branch meta learning approaches utilize a separate support branch

receiving the image of a designated object, to learn how to represent the objects' category and where to attend in the query image. Transfer learning approaches use a more simplified training scheme, by simply finetuning on the novel categories, often requiring freezing most of the detector weights.

After introducing the main concepts, we elaborated on how specific approaches differ from the general realization and gave short takeaways in order to highlight key insights for well performing methods. In particular, we identified the following trends: Additional loss functions should be incorporated for improving the intra- and inter-class variance for a better discrimination of categories. Dual-branch meta learning approaches benefit from attention-based aggregation methods. For transfer learning, it is helpful to incorporate techniques that allow to unfreeze more detector components during finetuning on novel classes.

Our analysis of benchmark results on the most widely used datasets PASCAL VOC and Microsoft COCO showed that both dual-branch meta learning and transfer learning approaches achieve superior results when proper methods are applied. It remains an open question which of these two concepts will prevail.

REFERENCES

- [1] Z. Q. Zhao, P. Zheng, S. T. Xu, and X. Wu, "Object detection with deep learning: A review," *IEEE Transactions on Neural Networks and Learning Systems (TNNLS)*, vol. 30, no. 11, pp. 3212–3232, 2019.
- [2] L. Liu, W. Ouyang, X. Wang, P. Fieguth, J. Chen, X. Liu, and M. Pietikäinen, "Deep Learning for Generic Object Detection: A Survey," *International Journal of Computer Vision (IJCV)*, vol. 128, pp. 261–318, 2020.
- [3] A. Katzmann, O. Taubmann, S. Ahmad, A. Mühlberg, M. Sühling, and H.-M. Groß, "Explaining clinical decision support systems in medical imaging using cycle-consistent activation maximization," *Neurocomputing*, vol. 458, pp. 141–156, 2021.
- [4] L. Mannocci, S. Villon, M. Chaumont, N. Guellati, N. Mouquet, C. Iovan, L. Vigliola, and D. Mouillot, "Leveraging social media and deep learning to detect rare megafauna in video surveys," *Conservation Biology*, 2021.
- [5] L. B. Smith, S. S. Jones, B. Landau, L. Gershkoff-Stowe, and L. Samuelson, "Object name learning provides on-the-job training for attention," *Psychological Science*, vol. 13, no. 1, pp. 13–19, 2002.
- [6] L. K. Samuelson and L. B. Smith, "They call it like they see it: Spontaneous naming and attention to shape," *Developmental Science*, vol. 8, no. 2, pp. 182–198, 2005.
- [7] L. A. Schmidt, "Meaning and compositionality as statistical induction of categories and constraints," Ph.D. dissertation, Massachusetts Institute of Technology, 2009.
- [8] H. Chen, Y. Wang, G. Wang, and Y. Qiao, "LSTD: A Low-Shot Transfer Detector for Object Detection," in *AAAI Conference on Artificial Intelligence (AAAI)*, 2018, pp. 2836–2843.
- [9] X. Yan, Z. Chen, A. Xu, X. Wang, X. Liang, and L. Lin, "Meta R-CNN: Towards general solver for instance-level low-shot learning," in *International Conference on Computer Vision (ICCV)*, 2019, pp. 9576–9585.
- [10] O. Vinyals, G. Deepmind, C. Blundell, T. Lillicrap, K. Kavukcuoglu, and D. Wierstra, "Matching Networks for One Shot Learning," in *Neural Information Processing Systems (NeurIPS)*, 2016, pp. 3630–3638.
- [11] J. Snell, K. Swersky, T. R. Zemel, and R. Zemel, "Prototypical Networks for Few-shot Learning," in *Conference on Neural Information Processing Systems (NeurIPS)*, vol. 30, 2017.
- [12] Y. Wang, J. T. Kwok, L. M. Ni, H. Kong, and Q. Yao, "Generalizing from a Few Examples: A Survey on Few-shot Learning," *ACM Computing Surveys (CSUR)*, vol. 53, pp. 1–34, 2020.
- [13] T. M. Hospedales, A. Antoniou, P. Micaelli, and A. J. Storkey, "Meta-Learning in Neural Networks: A Survey," *IEEE Transactions on Pattern Analysis and Machine Intelligence (TPAMI)*, 2021.
- [14] O. Chapelle, B. Scholkopf, and A. Zien, "Semi-supervised learning," *IEEE Transactions on Neural Networks (TNN)*, vol. 20, no. 3, pp. 542–542, 2010.
- [15] J. E. Van Engelen and H. H. Hoos, "A survey on semi-supervised learning," *Machine Learning (ML)*, vol. 109, no. 2, pp. 373–440, 2020.
- [16] P. Tang, C. Ramaiah, Y. Wang, R. Xu, C. Xiong, and S. Research, "Proposal Learning for Semi-Supervised Object Detection," in *IEEE Winter Conference on Applications of Computer Vision (WACV)*, 2021, pp. 2291–2301.
- [17] W. Liu, D. Anguelov, D. Erhan, C. Szegedy, S. Reed, C. Y. Fu, and A. C. Berg, "SSD: Single shot multibox detector," in *European Conference on Computer Vision (ECCV)*, 2016, pp. 21–37.
- [18] J. Redmon, S. Divvala, R. Girshick, and A. Farhadi, "You only look once: Unified, real-time object detection," in *IEEE Conference on Computer Vision and Pattern Recognition (CVPR)*, 2016, pp. 779–788.
- [19] J. Redmon and A. Farhadi, "YOLO9000: Better, faster, stronger," in *IEEE Conference on Computer Vision and Pattern Recognition (CVPR)*, 2017, pp. 6517–6525.
- [20] —, "Yolo3: An incremental improvement," *arXiv preprint arXiv:1804.02767*, 2018.
- [21] A. Bochkovskiy, C.-Y. Wang, and H.-Y. M. Liao, "Yolo4: Optimal speed and accuracy of object detection," *arXiv preprint arXiv:2004.10934*, 2020.
- [22] T. Y. Lin, P. Goyal, R. Girshick, K. He, and P. Dollár, "Focal Loss for Dense Object Detection," in *International Conference on Computer Vision (ICCV)*, vol. 42, 2017, pp. 318–327.
- [23] R. Girshick, J. Donahue, T. Darrell, and J. Malik, "Rich feature hierarchies for accurate object detection and semantic segmentation," in *IEEE Conference on Computer Vision and Pattern Recognition (CVPR)*, 2014, pp. 580–587.
- [24] R. Girshick, "Fast r-cnn," in *IEEE Conference on Computer Vision and Pattern Recognition (CVPR)*, 2015, pp. 1440–1448.
- [25] S. Ren, K. He, R. Girshick, and J. Sun, "Faster R-CNN: Towards real-time object detection with region proposal networks," in *Conference on Neural Information Processing Systems (NeurIPS)*, 2015.
- [26] K. He, X. Zhang, S. Ren, and J. Sun, "Deep Residual Learning for Image recognition," in *IEEE Conference on Computer Vision and Pattern Recognition (CVPR)*, 2016, pp. 770–778.
- [27] T.-Y. Lin, P. Dollár, R. Girshick, K. He, B. Hariharan, and S. Belongie, "Feature Pyramid Networks for Object Detection," in *IEEE Conference on Computer Vision and Pattern Recognition (CVPR)*, 2017, pp. 2117–2125.
- [28] A. Bansal, K. Sikka, G. Sharma, R. Chellappa, and A. Divakaran, "Zero-Shot Object Detection," in *European Conference on Computer Vision (ECCV)*, 2018, pp. 384–400.
- [29] S. Rahman, S. Khan, and F. Porikli, "Zero-Shot Object Detection: Learning to Simultaneously Recognize and Localize Novel Concepts," in *Asian Conference on Computer Vision (ACCV)*, 2018, pp. 547–563.
- [30] A. Gupta, P. Dollár, and R. Girshick, "Lvis: A Dataset for Large Vocabulary Instance Segmentation," in *IEEE Conference on Computer Vision and Pattern Recognition (CVPR)*, 2019, pp. 5351–5359.
- [31] Y. Zhang, B. Kang, B. Hooi, S. Yan, and J. Feng, "Deep long-tailed learning: A survey," *arXiv preprint arXiv:2110.04596*, 2021.
- [32] X. Hu, Y. Jiang, K. Tang, J. Chen, C. Miao, and H. Zhang, "Learning to Segment the Tail," in *IEEE Conference on Computer Vision and Pattern Recognition (CVPR)*, 2020, pp. 14 042–14 051.
- [33] D. Zhang, J. Han, G. Cheng, and M.-H. Yang, "Weakly supervised object localization and detection: A survey," *IEEE Transactions on Pattern Analysis and Machine Intelligence (TPAMI)*, 2021.
- [34] F. Shao, L. Chen, J. Shao, W. Ji, S. Xiao, L. Ye, Y. Zhuang, and J. Xiao, "Deep learning for weakly-supervised object detection and object localization: A survey," *arXiv preprint arXiv:2105.12694*, 2021.
- [35] A. Jaiswal, Y. Wu, P. Natarajan, and P. Natarajan, "Class-agnostic Object Detection," in *IEEE/CVF Winter Conference on Applications of Computer Vision (WACV)*, 2021, pp. 919–928.
- [36] M. Kaya and H. Ş. Bilge, "Deep metric learning: A survey," *Symmetry*, vol. 11, no. 9, p. 1066, 2019.
- [37] K. Q. Weinberger and L. K. Saul, "Distance Metric Learning for Large Margin Nearest Neighbor Classification," *Journal of Machine Learning Research (JMLR)*, vol. 10, pp. 207–244, 2009.
- [38] D. Aganjan, M. Eisenbach, J. Wagner, D. Seichter, and H.-M. Gross, "Revisiting loss functions for person re-identification," in *International Conference on Artificial Neural Networks (ICANN)*. Springer, 2021, pp. 30–42.
- [39] L. Zhang, S. Zhou, J. Guan, and J. Zhang, "Accurate Few-shot Object Detection with Support-Query Mutual Guidance and Hybrid Loss,"

- in *IEEE Conference on Computer Vision and Pattern Recognition (CVPR)*, 2021, pp. 14424–14432.
- [40] K. He, G. Gkioxari, P. Dollár, and R. Girshick, “Mask R-CNN,” *International Conference on Computer Vision (ICCV)*, pp. 2961–2969, 2017.
 - [41] Y. Xiao and R. Marlet, “Few-Shot Object Detection and Viewpoint Estimation for Objects in the Wild,” in *European Conference on Computer Vision (ECCV)*, 2020, pp. 192–210.
 - [42] A. Li and Z. Li, “Transformation Invariant Few-Shot Object Detection,” in *IEEE Conference on Computer Vision and Pattern Recognition (CVPR)*, 2021, pp. 3094–3102.
 - [43] B. Kang, Z. Liu, X. Wang, F. Yu, J. Feng, and T. Darrell, “Few-shot object detection via feature reweighting,” in *International Conference on Computer Vision (ICCV)*, 2019, pp. 8419–8428.
 - [44] B. Li, B. Yang, C. Liu, F. Liu, R. Ji, and Q. Ye, “Beyond Max-Margin: Class Margin Equilibrium for Few-shot Object Detection,” in *IEEE Conference on Computer Vision and Pattern Recognition (CVPR)*, 2021.
 - [45] L. Liu, B. Wang, Z. Kuang, J. H. Xue, Y. Chen, W. Yang, Q. Liao, and W. Zhang, “GenDet: Meta Learning to Generate Detectors From Few Shots,” *IEEE Transactions on Neural Networks and Learning Systems (TNNLS)*, pp. 1–13, 2021.
 - [46] Y. Li, W. Feng, S. Lyu, Q. Zhao, and X. Li, “MM-FSOD: Meta and metric integrated few-shot object detection,” *arXiv preprint arXiv:2012.15159*, pp. 1–30, 2020.
 - [47] T.-I. Chen, Y.-C. Liu, H.-T. Su, Y.-C. Chang, Y.-H. Lin, J.-F. Yeh, W.-C. Chen, and W. H. Hsu, “Dual-awareness Attention for Few-Shot Object Detection,” *IEEE Transactions on Multimedia (TMM)*, vol. 23, 2021.
 - [48] D.-J. Chen, H.-Y. Hsieh, and T.-L. Liu, “Adaptive Image Transformer for One-Shot Object Detection,” in *IEEE Conference on Computer Vision and Pattern Recognition (CVPR)*, 2021, pp. 12 247–12 256.
 - [49] Q. Fan, W. Zhuo, C.-K. Tang, and Y.-W. Tai, “Few-Shot Object Detection with Attention-RPN and Multi-Relation Detector,” in *IEEE Conference on Computer Vision and Pattern Recognition (CVPR)*, 2020, pp. 4013–4022.
 - [50] T.-i. Hsieh, Y.-c. Lo, H.-t. Chen, and T.-I. Liu, “One-Shot Object Detection with Co-Attention and Co-Excitation,” in *Conference on Neural Information Processing Systems (NeurIPS)*, 2019.
 - [51] C. Michaelis, M. Bethge, and A. S. Ecker, “Closing the Generalization Gap in One-Shot Object Detection,” *arXiv preprint arXiv:2011.04267*, pp. 1–13, 2020.
 - [52] G. Han, S. Huang, J. Ma, Y. He, and S.-F. Chang, “Meta Faster R-CNN: Towards Accurate Few-Shot Object Detection with Attentive Feature Alignment,” *arXiv preprint arxiv:2104.07719*, 2021.
 - [53] X. Li, L. Zhang, Y. P. Chen, Y.-W. Tai, and C.-K. Tang, “One-Shot Object Detection without Fine-Tuning,” *arXiv preprint arXiv:2005.03819*, 2020.
 - [54] G. Han, Y. He, S. Huang, J. Ma, and S.-F. Chang, “Query adaptive few-shot object detection with heterogeneous graph convolutional networks,” in *International Conference on Computer Vision (ICCV)*, 2021, pp. 3263–3272.
 - [55] H. Hu, S. Bai, A. Li, J. Cui, and L. Wang, “Dense Relation Distillation with Context-aware Aggregation for Few-Shot Object Detection,” in *IEEE Conference on Computer Vision and Pattern Recognition (CVPR)*, 2021.
 - [56] G. Kim, H.-G. Jung, and S.-W. Lee, “Few-Shot Object Detection via Knowledge Transfer,” in *IEEE International Conference on Systems, Man, and Cybernetics (SMC)*, 2020.
 - [57] G. Zhang, Z. Luo, K. Cui, and S. Lu, “Meta-DETR: Few-Shot Object Detection via Unified Image-Level Meta-Learning,” *arXiv preprint arXiv:2103.11731*, 2021.
 - [58] X. Zhu, T. Hospedales, and T. Xiang, “Incremental Few-Shot Object Detection,” in *IEEE Conference on Computer Vision and Pattern Recognition (CVPR)*, 2020.
 - [59] C. Michaelis, I. Ustyuzhaninov, M. Bethge, and A. S. Ecker, “One-Shot Instance Segmentation,” *arXiv preprint arXiv:1811.11507*, 2018.
 - [60] Y. Chen, X. Dai, M. Liu, D. Chen, L. Yuan, and Z. Liu, “Dynamic convolution: Attention over convolution kernels,” in *IEEE Conference on Computer Vision and Pattern Recognition (CVPR)*, 2020, pp. 11 030–11 039.
 - [61] F. Sung, Y. Yang, L. Zhang, T. Xiang, P. H. Torr, and T. M. Hospedales, “Learning to compare: Relation network for few-shot learning,” in *IEEE Conference on Computer Vision and Pattern Recognition (CVPR)*, 2018, pp. 1199–1208.
 - [62] X. Wang, R. Girshick, A. Gupta, and K. He, “Non-local Neural Networks,” in *IEEE Conference on Computer Vision and Pattern Recognition (CVPR)*, 2018, pp. 7794–7803.
 - [63] J. Hu, L. Shen, and G. Sun, “Squeeze-and-excitation networks,” in *IEEE Conference on Computer Vision and Pattern Recognition (CVPR)*, 2018, pp. 7132–7141.
 - [64] A. Vaswani, N. Shazeer, N. Parmar, J. Uszkoreit, L. Jones, A. N. Gomez, Ł. Kaiser, and I. Polosukhin, “Attention Is All You Need,” in *Conference on Neural Information Processing Systems (NeurIPS)*, 2017.
 - [65] T. N. Kipf and M. Welling, “Semi-supervised classification with graph convolutional networks,” in *International Conference on Learning Representations (ICLR)*, 2017.
 - [66] A. Li, W. Huang, X. Lan, J. Feng, Z. Li, and L. Wang, “Boosting few-shot learning with adaptive margin loss,” in *IEEE Conference on Computer Vision and Pattern Recognition (CVPR)*, 2020, pp. 12 576–12 584.
 - [67] J. Pennington, R. Socher, and C. D. Manning, “Glove: Global vectors for word representation,” in *Conference on Empirical Methods in Natural Language Processing (EMNLP)*, 2014, pp. 1532–1543.
 - [68] X. Zhou, D. Wang, and P. Krähenbühl, “Objects as Points,” *arXiv preprint arXiv:1904.07850*, 2019.
 - [69] Z. Tian, C. Shen, H. Chen, and T. He, “FCOS: Fully convolutional one-stage object detection,” in *International Conference on Computer Vision (ICCV)*, 2019, pp. 9627–9636.
 - [70] X. Zhu, W. Su, L. Lu, B. Li, X. Wang, J. Dai, and S. Research, “Deformable DETR: Deformable Transformers for End-to-End Object Detection,” in *International Conference on Learning Representations (ICLR)*, 2021.
 - [71] Z. Liu, Y. Lin, Y. Cao, H. Hu, Y. Wei, Z. Zhang, S. Lin, and B. Guo, “Swin Transformer: Hierarchical Vision Transformer using Shifted Windows,” *arXiv preprint arXiv:2103.14030*, 2021.
 - [72] H. Zhao, J. Shi, X. Qi, X. Wang, and J. Jia, “Pyramid Scene Parsing Network,” in *IEEE Conference on Computer Vision and Pattern Recognition (CVPR)*, 2017.
 - [73] L. Karlinsky, J. Shtok, S. Harary, E. Schwartz, A. Aides, R. Feris, R. Giryes, and A. M. Bronstein, “RepMet: Representative-based metric learning for classification and few-shot object detection,” in *IEEE Conference on Computer Vision and Pattern Recognition (CVPR)*, 2019, pp. 5192–5201.
 - [74] Y. Yang, F. Wei, M. Shi, and G. Li, “Restoring negative information in few-shot object detection,” in *Conference on Neural Information Processing Systems (NeurIPS)*, 2020.
 - [75] G. Zhang, K. Cui, R. Wu, S. Lu, and Y. Tian, “PNPDet : Efficient Few-shot Detection without Forgetting,” in *Winter Conference on Applications of Computer Vision (WACV)*, 2021, pp. 3823–3832.
 - [76] Y. X. Wang, D. Ramanan, and M. Hebert, “Meta-Learning to Detect Rare Objects,” in *International Conference on Computer Vision (ICCV)*, 2019, pp. 9924–9933.
 - [77] S. Li, W. Song, S. Li, A. Hao, and H. Quin, “Meta-RetinaNet for Few-shot Object Detection,” in *British Machine Vision Conference (BMVC)*, 2020.
 - [78] K. Fu, T. Zhang, Y. Zhang, M. Yan, Z. Chang, Z. Zhang, and X. Sun, “Meta-SSD: Towards Fast Adaptation for Few-Shot Object Detection with Meta-Learning,” *IEEE Access*, vol. 7, pp. 77 597–77 606, 2019.
 - [79] X. Wang, T. E. Huang, T. Darrell, J. E. Gonzalez, and F. Yu, “Frustratingly Simple Few-Shot Object Detection,” in *International Conference on Machine Learning (ICML)*, 2020.
 - [80] B. Sun, B. Li, S. Cai, Y. Yuan, and C. Zhang, “FSCE: Few-Shot Object Detection via Contrastive Proposal Encoding,” in *IEEE Conference on Computer Vision and Pattern Recognition (CVPR)*, 2021.
 - [81] W. Zhang, Y.-X. Wang, and D. A. Forsyth, “Cooperating RPN’s Improve Few-Shot Object Detection,” *arXiv preprint arXiv:2011.10142*, pp. 1–10, 2020.
 - [82] Z. Fan, Y. Ma, Z. Li, and J. Sun, “Generalized Few-Shot Object Detection without Forgetting,” in *IEEE Conference on Computer Vision and Pattern Recognition (CVPR)*, 2021.
 - [83] Z. Yang, Y. Wang, X. Chen, J. Liu, and Y. Qiao, “Context-Transformer: Tackling Object Confusion for Few-Shot Detection,” in *AAAI Conference on Artificial Intelligence (AAAI)*, 2020.
 - [84] W. Zhang and Y.-X. Wang, “Hallucination Improves Few-Shot Object Detection,” in *IEEE Conference on Computer Vision and Pattern Recognition (CVPR)*, 2021.
 - [85] J. Wu, S. Liu, D. Huang, and Y. Wang, “Multi-Scale Positive Sample Refinement for Few-Shot Object Detection,” in *European Conference on Computer Vision (ECCV)*, 2020, pp. 456–472.

- [86] A. Wu, S. Zhao, C. Deng, and W. Liu, "Generalized and Discriminative Few-Shot Object Detection via SVD-Dictionary Enhancement," in *Neural Information Processing Systems (NeurIPS)*, 2021.
- [87] A. Wu, Y. Han, L. Zhu, and Y. Yang, "Universal-prototype enhancing for few-shot object detection," in *International Conference on Computer Vision (ICCV)*, 2021, pp. 9567–9576.
- [88] L. Qiao, Y. Zhao, Z. Li, X. Qiu, J. Wu, and C. Zhang, "Defrcn: Decoupled faster r-cnn for few-shot object detection," in *International Conference on Computer Vision (ICCV)*, 2021, pp. 8681–8690.
- [89] Y. Li, H. Zhu, Y. Cheng, and W. Wang, "Few-Shot Object Detection via Classification Refinement and Distractor Retreatment," in *IEEE Conference on Computer Vision and Pattern Recognition (CVPR)*, 2021, pp. 15 395–15 403.
- [90] Y. Cao, J. Wang, Y. Jin, T. Wu, K. Chen, Z. Liu, and D. Lin, "Few-Shot Object Detection via Association and Discrimination," in *Conference on Neural Information Processing Systems (NeurIPS)*, 2021.
- [91] S. Khandelwal, R. Goyal, and L. Sigal, "UniT: Unified Knowledge Transfer for Any-shot Object Detection and Segmentation," in *IEEE Conference on Computer Vision and Pattern Recognition (CVPR)*, 2021.
- [92] C. Zhu, F. Chen, U. Ahmed, Z. Shen, and M. Savvides, "Semantic Relation Reasoning for Shot-Stable Few-Shot Object Detection," in *IEEE Conference on Computer Vision and Pattern Recognition (CVPR)*, 2021.
- [93] H. Xu, X. Wang, F. Shao, B. Duan, and P. Zhang, "Few-Shot Object Detection via Sample Processing," *IEEE Access*, pp. 29 207–29 221, 2021.
- [94] X. Chen, M. Jiang, and Q. Zhao, "Leveraging Bottom-Up and Top-Down Attention for Few-Shot Object Detection," *arXiv preprint arXiv:2007.12104*, pp. 1–12, 2020.
- [95] H. Qi, M. Brown, and D. G. Lowe, "Low-shot learning with imprinted weights," in *IEEE Conference on Computer Vision and Pattern Recognition (CVPR)*, 2018, pp. 5822–5830.
- [96] X. Chen, Y. Wang, J. Liu, and Y. Qiao, "Did: Disentangling-imprinting-distilling for continuous low-shot detection," *IEEE Transactions on Image Processing (TIP)*, vol. 29, pp. 7765–7778, 2020.
- [97] G. A. Miller, "Wordnet: a lexical database for english," *Communications of the ACM*, vol. 38, no. 11, pp. 39–41, 1995.
- [98] J. Deng, J. Guo, N. Xue, and S. Zafeiriou, "Arcface: Additive angular margin loss for deep face recognition," in *IEEE Conference on Computer Vision and Pattern Recognition (CVPR)*, 2019, pp. 4690–4699.
- [99] J. Zhang and S. Sclaroff, "Saliency detection: A boolean map approach," in *International Conference on Computer Vision (ICCV)*, 2013, pp. 153–160.
- [100] M. Cornia, L. Baraldi, G. Serra, and R. Cucchiara, "Predicting human eye fixations via an lstm-based saliency attentive model," *IEEE Transactions on Image Processing (TIP)*, vol. 27, no. 10, pp. 5142–5154, 2018.
- [101] H. Zhang, J. Xue, and K. Dana, "Deep ten: Texture encoding network," in *IEEE Conference on Computer Vision and Pattern Recognition (CVPR)*, 2017, pp. 708–717.
- [102] K. Wang, J. H. Liew, Y. Zou, D. Zhou, and J. Feng, "Panet: Few-shot image semantic segmentation with prototype alignment," in *International Conference on Computer Vision (ICCV)*, 2019, pp. 9197–9206.
- [103] J. Liu, L. Song, and Y. Qin, "Prototype rectification for few-shot learning," in *European Conference on Computer Vision (ECCV)*, 2020, pp. 741–756.
- [104] M. Everingham, L. Van Gool, C. K. Williams, J. Winn, and A. Zisserman, "The Pascal Visual Object Classes (VOC) Challenge," *International Journal of Computer Vision (IJCV)*, vol. 88, no. 2, pp. 303–338, 2010.
- [105] T.-Y. Lin, M. Maire, S. Belongie, J. Hays, P. Perona, D. Ramanan, P. Dollár, and C. L. Zitnick, "Microsoft COCO: Common Objects in Context," in *European Conference on Computer Vision (ECCV)*, 2014, pp. 740–755.
- [106] O. Russakovsky, J. Deng, H. Su, J. Krause, S. Satheesh, S. Ma, Z. Huang, A. Karpathy, A. Khosla, M. Bernstein, A. C. Berg, and L. Fei-Fei, "ImageNet Large Scale Visual Recognition Challenge," *International Journal of Computer Vision (IJCV)*, pp. 211–252, 2015.
- [107] A. Kuznetsova, H. Rom, N. Alldrin, J. Uijlings, I. Krasin, J. Pont-Tuset, S. Kamali, S. Popov, M. Mallocci, A. Kolesnikov *et al.*, "The open images dataset v4," *International Journal of Computer Vision (IJCV)*, vol. 128, no. 7, pp. 1956–1981, 2020.
- [108] L. Karlinsky, J. Shtok, A. Alfassy, M. Lichtenstein, S. Harary, E. Schwartz, S. Doveh, P. Sattigeri, R. Feris, A. Bronstein, and R. Giryes, "StarNet: towards Weakly Supervised Few-Shot Object Detection," in *AAAI Conference on Artificial Intelligence (AAAI)*, 2021, pp. 1743–1753.
- [109] Z. Fan, J.-G. Yu, Z. Liang, J. Ou, C. Gao, G.-S. Xia, and Y. Li, "Fgn: Fully guided network for few-shot instance segmentation," in *IEEE Conference on Computer Vision and Pattern Recognition (CVPR)*, 2020, pp. 9172–9181.
- [110] K. Nguyen and S. Todorovic, "Fapis: A few-shot anchor-free part-based instance segmenter," in *IEEE Conference on Computer Vision and Pattern Recognition (CVPR)*, 2021, pp. 11 099–11 108.

APPENDIX

Faster R-CNN

As a lot of approaches for few-shot object detection build upon Faster R-CNN, its architecture is depicted in Figure 11 and further described in the following: First, features are

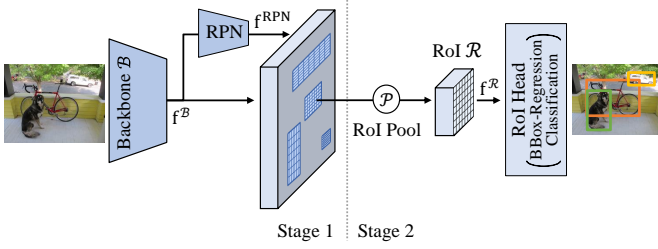


Fig. 11: Architecture of Faster R-CNN [25]

extracted in a backbone network \mathcal{B} such as a ResNet [26]. Afterwards, a region proposal network (RPN) predicts bounding box parameters for region proposals. Therefore, anchor boxes of different aspect ratios are used which are placed all over the feature maps and encode all possible object locations. The RPN's binary classifier predicts whether an anchor box is a foreground object, or whether it will be discarded as background. Moreover, the RPN also regresses anchor deltas to better adjust the anchor boxes to the objects. The foreground objects are then considered as region proposals and can contain arbitrary objects. In the second stage, RoI Pooling uses the predicted bounding box parameters for cropping regions of the backbone's output feature maps. These pooled regions are referred to as regions of interests (RoIs). RoI Pooling as well as its advanced method RoI Align [40] are configured such that all RoIs have the same spatial resolution (typically 7×7). Finally, the box head classifies the RoIs into the object categories (+ one additional background category) and the bounding box parameters are further refined.

For higher detection rates, the backbone is often extended with a feature pyramid network (FPN) [27] as illustrated in Fig. 12. The FPN outputs feature maps of different resolutions which helps the detector in detecting objects of different sizes. When a FPN is used, the RPN is applied once for each feature scale. Depending on the size of the region proposal a corresponding feature scale is used for RoI Pooling.

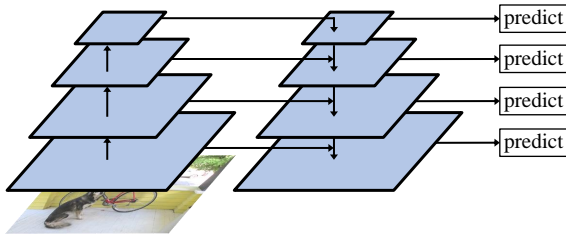


Fig. 12: Feature pyramid network (FPN) [27]

Mathematical notation

The following listing of mathematical identifiers is intended to serve as a reference.

\mathcal{C}_{base}	base categories
\mathcal{C}_{novel}	novel categories
\mathcal{D}_{base}	base dataset
\mathcal{D}_{novel}	novel dataset
$f^{\mathcal{B}}$	backbone features
f^{RPN}	features after RPN
$f^{\mathcal{R}}$	features of the RoI
\mathcal{R}	RoI
$I^{\mathcal{Q}}$	query image
$I^{\mathcal{S}}$	support image
$I^{\mathcal{S},c}$	support image of category c
\mathcal{Q}	query branch
\mathcal{S}	support branch
$f^{\mathcal{Q}}$	query features
$f^{\mathcal{S}}$	support features
$f^{\mathcal{S},c}$	support features of category c
\mathcal{B}	backbone
$f^{\mathcal{Q},\mathcal{B}}$	features after query backbone
$f^{\mathcal{S},\mathcal{B}}$	features after support backbone
\mathcal{R}^c	RoI of category c
\mathcal{A}	aggregation
$\mathcal{R}^{\mathcal{A}}$	RoI after aggregation
$\mathcal{R}^{\mathcal{A},c}$	RoI after aggregation of category c
K	number of shots
N	number of novel categories
\mathcal{M}_{init}	initial model (pretrained on imagenet)
\mathcal{M}_{base}	model trained on \mathcal{D}_{base}
\mathcal{M}_{final}	model trained on \mathcal{D}_{novel} and maybe \mathcal{D}_{base}

Scope of this survey

In Fig. 13 we list the approaches, that we cover in this survey. First of all, we can see that few-shot object detection is a rather young but emerging research field as most approaches have been published only within the last two years. Most approaches use transfer learning or dual-branch meta learning. We include unpublished preprints on arxiv from the last two years, as we expect them to be published in the near future.

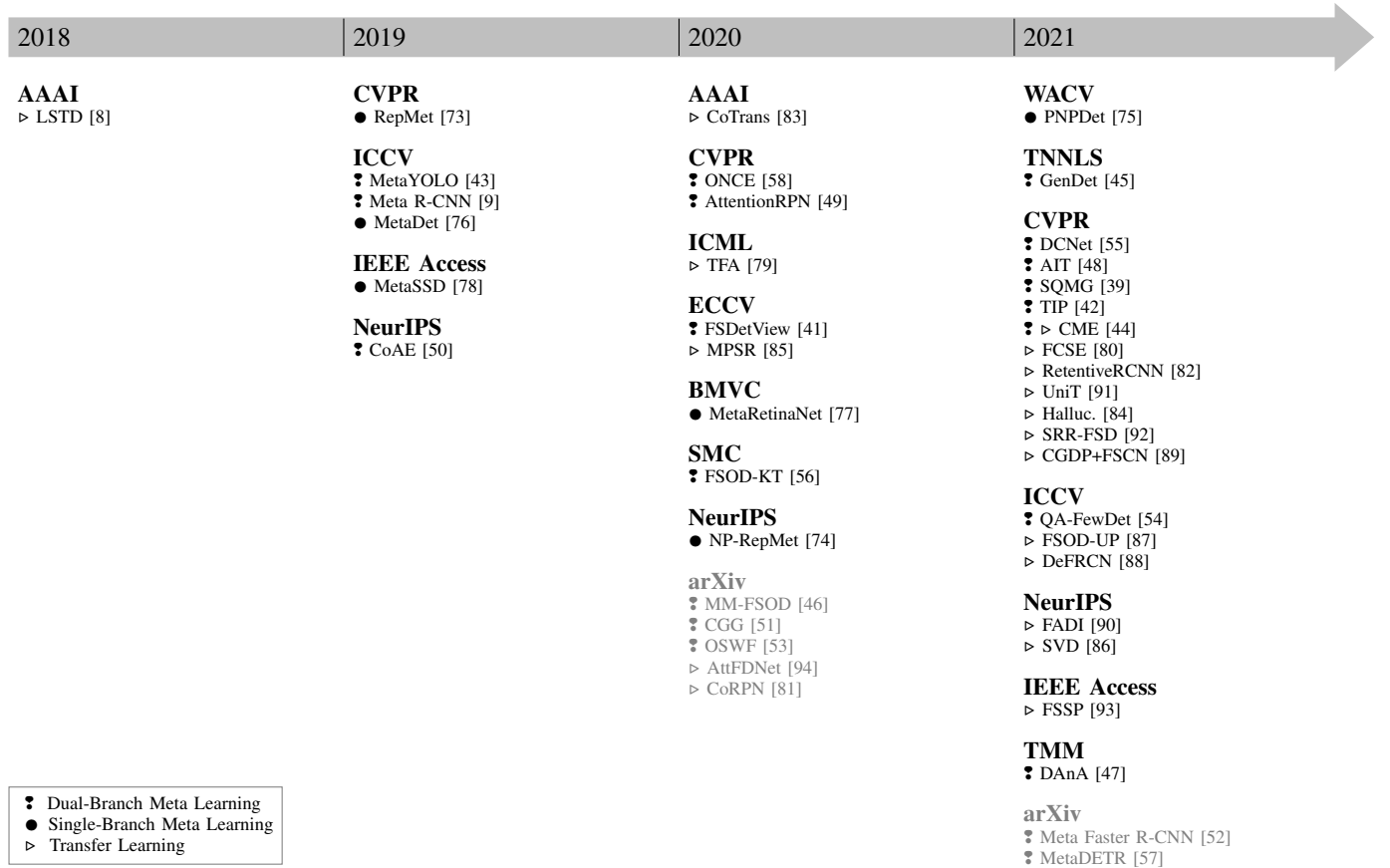


Fig. 13: Scope of this survey. We categorize approaches into dual- and single-branch meta learning and transfer learning.